Simple solutions for downslope pipeline walking on elastic-perfectly-plastic soils

Adriano Castelo
PhD Candidate, The University of Western Australia
UWA (M053), 35 Stirling Highway CRAWLEY WA 6009, Australia
21445298@student.uwa.edu.au
ASME Student Member

David White
Professor, The University of Western Australia
UWA (M053), 35 Stirling Highway CRAWLEY WA 6009, Australia
david.white@uwa.edu.au

Yinghui Tian
Professor, The University of Western Australia
UWA (M053), 35 Stirling Highway CRAWLEY WA 6009, Australia
yinghui.tian@uwa.edu.au

ABSTRACT

Pipeline Walking is a phenomenon that occurs when High Pressure and High Temperature pipelines experience axial instability over their operational lifetime, and migrate globally in one direction. Existing analytical solutions treat the axial soil response as rigid-plastic but this does not match the response observed in physical model tests. In this paper, the authors develop a new analytical strategy using elastic-perfectly-plastic axial pipe-soil interaction, which leads to more realistic walking rate predictions. The new analytical methodology is benchmarked with a series of Finite Element Analyses (FEA), which constitutes a parametric study performed to test the proposed expressions and improve on the understanding of the influence of axial mobilisation distance.

KEYWORDS

axial resistance; pipe-soil interaction; pipeline walking; finite-element modelling; offshore engineering

1 INTRODUCTION

Offshore pipelines are becoming increasingly important as hydrocarbon sources become more difficult to reach. The global stability of these pipelines in response to operational loading is a critical issue for the design of oil and gas projects. Such stability comprises the actions of hydrodynamic loads and the effects of expansion and contraction triggered by the High-Pressure and High-Temperature (HPHT) operational conditions (usually imposed by frontier reservoirs), which both constitute the major focus of geotechnical design for pipelines.

The stability of offshore pipelines is also impacted by the slope of the seabed. New hydrocarbon sources are commonly located in regions with noticeable depth variations, in deep water far from shore. These operational conditions are particularly common in the Gulf of Mexico and Northwest Australia, which are currently in operation, and others that are in development, such as the Brazilian Pre-Salt and the Arctic Area.

Threats to the integrity of offshore pipelines by the combination of HPHT conditions and a sloping seabed were first observed by [1]. Later, industry-supported research documented many cases of “axial creeping” now known as the “Pipeline Walking”, as per [2].

Four mechanisms have been found to incite pipeline walking, as per [3]:

1. Tension at the end of the flowline;
2. Thermal transients along the line;
3. Multiphase fluid behaviour during restart operations;

4. Seabed slopes along the pipeline route.

Each of the four mechanisms creates an asymmetry in the profile of Effective Axial Force (EAF). This asymmetry generally results in pipeline walking, by causing unequal pipeline displacements during cycles of loading and unloading. This paper focuses on the fourth mechanism.

When pipelines are subjected to changes in temperature and pressure, pipeline walking can occur. During the Start-Up (SUp) phase, temperature and pressure increments cause the pipelines to expand axially. This expansion is resisted by the pipe-soil interaction forces which results in effective compression of the pipeline. When pipelines are submitted to temperature and pressure reductions in the Shutdown (SDown) phase, effective tension is induced in the pipeline.

For "long" pipelines, the effective compression build up occurs along a sufficient length to induce enough mechanical strain to fully compensate for the thermo-mechanical expansion during the hot stages. For "short" pipelines, the compression build up, due to soil resistance, is not sufficient to fully compensate for the expansion.

When "short" pipelines are located on a sloping seabed and are not anchored, cycles of expansion and contraction may cause the pipelines to move with geometric asymmetries between the start-up and shutdown phases. The sloping seabed generates a component of weight to act parallel with the seabed in a downslope direction.

Even if pipeline walking is not a limit state in itself, it may present several design challenges, which include:

- Overstressing of end connections (and in-line connections);

- Loss of tension in a steel catenary riser;
- Increased loading leading to lateral buckling;
- Route instability (curve pull out);
- Need for anchoring mitigation.

Therefore, pipeline walking must be avoided since its consequences may create downtime and environmental risk, as pointed out by [1].

It is known that pre-operational phases may influence the soil resistance during the operational lifetime of a pipeline through the pre-operational embedment. As noticed by [4], typical pipeline embedments can increase the soil axial resistance by 10-20%. This study considers a range of axial resistance so the results cover the range of conditions that could be created by different values of embedment. In practice, the soil resistance may vary during the pipeline life, in which case the walking rate will also vary as a result of this. The authors would like to clarify that the suggested solutions also apply in cases of varying resistance during the field life requiring only an update on the assessments' inputs.

In this paper, focusing exclusively on the seabed slope mechanism, the authors develop a new analytical strategy extending the traditional solution, which uses a Rigid-Plastic (RP) soil idealization, to a new set of formulations accounting for the Elastic-Perfectly-Plastic (EP) soil behaviour, which is a simple pipe-soil interaction model [5]. A parametric study is developed with the help of a Finite Element Analysis (FEA) set, which will serve as proof for the proposed set of new equations, leading to more realistic walking rate predictions.

2 BACKGROUND TO PIPELINE WALKING

Different papers have been published on pipeline walking in the last two decades. Nearly all publications found on this topic are very site-specific [6] and [7], with few exceptions providing generalizations and broad guidance on this issue [2], [3] and [8].

When the downslope mechanism is taken into consideration the effective axial force plot demonstrates the asymmetry, as referred in section 1 and shown in Fig. 1, for three operational loading cycles. This asymmetry, which accounts for the weight component action, controls the offset distance X_{ab}, which is the distance between the Virtual Anchor Sections (VAS) as defined by [2]. X_{ab} is also present in the different profiles of Axial Displacement, δ_x, as shown by Fig. 2. In Fig. 2, the axial displacements are shown for the same three operational cycles shown in Fig. 1, throughout the entire pipeline length. In addition, Fig. 2 also provides a detailed progression of the VAS transition along the three operational cycles considered. More attention is given to X_{ab} in latter part of this paper.

So far pipeline walking has been dealt with through a series of equations which account for a rigid-plastic soil response. In this paper, an extended version of the analytical solution is described for elastic-perfectly-plastic soil behaviour.

Fig. 3 provides a schematic view of the Force - Displacement curve (FxD) for a given non-linear soil. It also accounts for rigid-plastic resistance behaviour and presents two different elastic-perfectly-plastic approaches – commonly used as ideal representations for the real non-linear soil. While the magnitude of the limiting axial resistance depends on soil strength, pipe roughness and drainage conditions [9], these effects are beyond the scope of the present study. Instead, the focus of this paper work is the influence of mobilisation distance, δ_{mob}, on the pipeline walking phenomenon.

The pipe-soil interaction varies with many different properties, [10]. Since this paper simplifies the pipe-soil interaction as an elastic-perfectly-plastic [5], it is simpler to treat the mobilisation displacement as an independent parameter, which allows covering the full parameter space for a wider range of soils. The authors acknowledge that different techniques might be used to obtain the pipe-soil interaction model, but these are not part of this paper scope.

Two different elastic-perfectly-plastic fits are shown in Fig. 3. One is a “Stiff Fit” in which the mobilisation distance is denoted $\delta_{mobStiff}$. The other is a more compliant case, “Soft Fit”, in which the mobilisation distance is denoted $\delta_{mobSoft}$. In this paper, the mobilisation distances differ by a factor of 3.33, and span the typical range of plausible elastic-perfectly-plastic fits. This is a typical uncertainty range for the non-linear response observed in model tests of axial pipe-soil interaction. Typically, $\delta_{mobStiff}$ and $\delta_{mobSoft}$ differ by a factor of up to 5, [9].

Fig. 3 brings to light two derived parameters that are explored in the finite element analyses parametric study (section 10): Load and Unload-Reload Areas (the shaded areas presented for the Soft Fit only). They represent the area loss between rigid-plastic and elastic-perfectly-plastic resistance approaches in terms of the FxD curves. They are very useful for the “elastic correction” explanation developed later.

During a reversal in the mobilised friction, the displacement required to reach the limiting resistance in the opposite direction is $2\delta_{mob}$, and the unloading stiffness matches the loading stiffness.

3 PROBLEM DEFINITION

To illustrate the behaviour involved in downslope pipeline walking, the properties of a typical example are given in Table 1. General properties, such as temperature loads and geometric data are in keeping with the values presented in Table 1, to allow the results to be applied more broadly in the future.

4 RIGID-PLASTIC ANALYTICAL SOLUTIONS

The current design practice – in accordance with [8] – involves three different calculation steps to analytically assess pipeline walking rate under the influence of seabed slope.

The first calculation step assesses the distance between the VASs, $X_{ab,RP}$, as presented by Fig. 1:

$$X_{ab,RP} = \frac{L \tan \beta}{\mu} \quad \textbf{(1)}$$

The second calculation step assesses the change in force in the pipeline, $\Delta S_{S,RP}$, between start-up and shutdown phases over the length of the pipeline denoted by $X_{ab,RP}$:

$$\Delta S_{S,RP} = -WL(\mu \cos \beta - |\sin \beta|) \quad \textbf{(2)}$$

This change in force, occurring over the distance $X_{ab,RP}$, creates the asymmetry in axial movement of the pipeline over a single temperature cycle, which is the origin of the walking behaviour. The walking distance per cycle, WR_{RP} can then be determined in the third and last step by combining equations (1) and (2):

$$WR_{RP} = \frac{[|\Delta P| + WL|\sin\beta| - WL\mu\cos\beta]L\tan\beta}{EA\mu} \tag{3}$$

where ΔP is the change in fully constrained force, as per [2].

However, equation (3) can be entirely rewritten as:

$$WR_{RP} = \frac{(\Delta S_{S,RP} - \Delta P)X_{ab,RP}}{EA} \tag{4}$$

Equation (4) might also be rewritten more fundamentally as:

$$WR_{RP} = -\frac{1}{EA}\left(\int_{VAS_{SDown,RP}}^{VAS_{SUp,RP}} (\Delta P)dx - \int_{VAS_{SDown,RP}}^{VAS_{SUp,RP}} (\Delta S_s)dx\right) \tag{5}$$

The rigid-plastic soils equation (2) is equal to $\Delta S_{S,RP}$ integral (see Appendix A for additional steps in this analysis).

The analytical solutions shown above – equations (1), (2), (3), (4) and (5) – have been used to calculate pipeline walking rates based on the rigid-plastic assumption. Table 2 summarizes the analytical results for [8] based on the general pipeline properties given in Table 1.

5 FINITE ELEMENT ANALYSES METHODOLOGY

The finite element model used for this paper was a simplified model of a straight pipeline laid on a uniformly sloping seabed using the parameters presented in Table 1.

The pipeline was represented by 5001 nodes connected by 5000 equal Euler Bernoulli beams (B33 elements in Abaqus) representing the 5000m long pipeline. Each element, therefore, is 1 metre in length.

The pipe-soil interaction was modelled as elastic-perfectly-plastic spring-slider elements connected to each pipeline node. The spring-slider elements were developed as User Elements (UELs) described by a subroutine in FORTRAN.

Fig. 4 shows an overall sketch of the finite element model. It presents the uniformly sloped pipeline and provides information about the boundary conditions imposed to all nodes, which can only displace along the local longitudinal axis given the UEL reaction.

The spring-slider provided a constant stiffness between zero and a certain prescribed displacement (mobilisation distance) and a corresponding force (according to Hooke's law). If the displacement level exceeds the mobilisation distance, the UEL provides zero tangent stiffness and a constant force, as per the plastic plateau. On reversal, the same stiffness is considered, until the resultant force equals the plastic plateau.

The UEL behaviour shown in Fig. 3 is presented in terms of the loads normal to the seabed.

This paper considers only weight and temperature as the loads acting on the pipeline. Pressure was disregarded since it can be equally represented by an extra temperature load [11].

The effect of the uniform slope is considered as an axial or longitudinal load equivalent to the component of the pipeline weight, as given by:

$$W_{comp} = W \sin \beta \quad \textbf{(6)}$$

The temperature loads were considered by temperature increments applied directly to the pipeline. Operational cycling was performed taking into account the steady operational profile (start-up) and the rest condition (shutdown).

The analyses were performed by:

1. Generating pipeline (nodes and elements) geometry;
2. Applying boundary conditions and UEL properties;
3. Applying gravity to pipeline;
4. Applying temperature increment (start-up temperature);
5. Applying temperature decrement (shutdown temperature);
6. Iterating phases 4 and 5 (9 times);
7. Extracting results from simulations' outputs.

6 FINITE ELEMENT ANALYSES COMPARISON WITH RIGID-PLASTIC SOLUTION

Fig. 5 presents the effective axial force responses for the EP Stiff and the Soft fits; while Fig. 6 and Fig. 7 present the δ_x plots for the EP Stiff Fit and the EP Soft Fit, respectively.

From the rigid-plastic case [3], the zero displacement point is exactly the same as the maximum effective axial force point (Table 3). However, the elastic-perfectly-plastic FE results show that the point of zero displacement no longer coincides with the point of maximum effective axial force.

As defined by [2], the VASs are the sections where the δ_x is zero and for the rigid-plastic soil response the VAS and the point of highest effective axial force coincide, which makes the solution proposed by [8] perfectly applicable for rigid-plastic soils.

However, elastic-perfectly-plastic soil behaviour complicates the X_{ab} definition, as used by [3] and [8]. Thus, X_{ab} needs to be redefined. In addition, the points on the pipe with zero net movement (δ_x=0) over the period of temperature change (either start-up or shutdown) are not stationary over this period but they move initially in one direction then return to their original position. Here, these sections with zero net movement are called "Stationary Points" (SP). While δ_x during the temperature change phase is ideally zero for these sections, in fact they move through a cycle of displacement and return to the original position at the end of the expansion or contraction. Fig. 8 shows the mentioned behaviour for stationary points during some load phases (for the EP Stiff Fit) along with a schematic plot of the finite element model to clarify the location of these stationary points. It is important to highlight that there will be one stationary point per loading phase, which will remain at the same pipeline Kilometre Post (KP), represented by the model nodes, as long as the conditions (temperature, soil, geometry, etc.) also remain the same during the operational lifetime.

In the following analysis, X_{ab} is defined as the distance between the stationary points. This definition is more useful than the distance between the maxima in the effective axial force profiles because the walking rate per cycle is fundamentally related to the integrated change in effective axial force in the length of pipe between the stationary points.

7 X_{ab} FOR ELASTIC-PERFECTLY-PLASTIC SOIL

The three different values for X_{ab} ($X_{ab,RP}$, X_{ab,EP_Stiff} *and* X_{ab,EP_Soft}) are compared to δ_{mob}, in Fig. 9, which shows the linear dependence of X_{ab} on δ_{mob}. Imagining there is a certain level of mobilisation distance which makes X_{ab} to be equal to zero (and consequently ceases the walking pattern), represented by δ_{null}, which will be given later in this paper, the following linear equation might be written:

$$X_{ab,EP} = X_{ab,RP}\left(1 - \frac{\delta_{mob}}{\delta_{null}}\right) \tag{7}$$

This definition of $X_{ab,EP}$ for use in equation (4) is now defined for elastic-perfectly-plastic soils, there is only one other missing – $\Delta S_{S,EP}$ – in order for the elastic-perfectly-plastic walking rate be derived analytically.

8 ΔS_S FOR ELASTIC-PERFECTLY-PLASTIC SOIL

For rigid-plastic soils, ΔS_S can be obtained directly from the basic problem parameters using equation (2). For elastic-perfectly-plastic soils, however, ΔS_S is not straight forward, as the effective axial force profile is not triangular. For this reason, the effective axial force equations need to be redefined by adopting the solution for an elastic column compressed within an elastic medium, as used in the analysis of piles. This leads to a second order linear differential equation which represents the displacement, δ, along the longitudinal axis, x, as shown by equation (8) from [12].

$$\delta = K_1 e^{\xi x} + K_2 e^{-\xi x} \tag{8}$$

where K_1 and K_2 are arbitrary constants, and ξ is exponential factor. More detail about these parameters is given in Appendix B.

However, before solving the differential equation the boundary conditions among the different behaviour patterns along the pipe route need to be defined.

Table 4 presents the physical boundaries that should be considered for the elastic-perfectly-plastic effective axial force calculation, which segregates the different zones of the pipeline. For pipeline zones *Z1* and *Z4* effective axial force is equivalent to the rigid-plastic solution with straight line behaviour and constant gradient – equations (9) and (10):

$$W(\mu\cos\beta + \sin\beta) \tag{9}$$
$$W(\mu\cos\beta - \sin\beta) \tag{10}$$

In contrast to zones *Z1* and *Z4*, the behaviour of the *Z2* and *Z3* central zones (in the vicinity of the highest effective axial force section), creates two different parabolic curves (within the effective axial force plot), whose gradients vary from 0 to the values given by equations (9) and (10).

Fig. 10 presents a schematic plot accounting the physical boundaries and also the revised solution for a hypothetic case.

i δ_x Boundary Conditions

Considering the physical boundaries and their outcomes in terms of displacement, δ, it is clear that displacements at x_{23} are zero, while at x_{12} and x_{34} displacements are equal to δ_{mob}, where the soil resistance is fully mobilised.

ii Effective Axial Force Boundary Conditions

From Fig. 10 it is clear that some boundary conditions must be respected when obtaining the analytical elastic-perfectly-plastic effective axial force response; which are:

- Continuity of slope for the three zone boundaries;
- Continuity of effective axial force at the three zone boundaries.

These effective axial force boundary conditions might be rewritten as shown in Table 5. The question mark in Table 5 might only be answered after the differential equation is solved and an expression for the effective axial force calculation is reached.

Hence, a general equation was written as follows:

$$\left(\frac{dF}{dx}\right)_x = \begin{cases} \mu W_{Z1}, & \delta_x \leq -\delta_{mob} \\ \left(\dfrac{\mu W_{Z1}}{\delta_{mob}}\right)\delta_x, & -\delta_{mob} < \delta_x < 0 \\ \left(\dfrac{\mu W_{Z4}}{\delta_{mob}}\right)\delta_x, & 0 < \delta_x < \delta_{mob} \\ \mu W_{Z4}, & \delta_x \geq \delta_{mob} \end{cases} \tag{11}$$

where $\mu W_{Z?}$ represents the soil resistance plus or minus, depending on the zone considered, the weight component acting on the pipe due to the seabed slope.

iii Effective Axial Force Pipe Differential Equation

Observing the effective axial force boundary conditions and their implications, the effective axial force differential equation could be written as:

$$EAF_{(x)} = \begin{cases} \mu W_{Z1} * x, \quad 0 \leq x \leq x_{12} \\ EAF_{(x_{12})} + \sqrt{\dfrac{EA\mu W_{Z1}}{\delta_{mob}}}\left[K_{1(x)}\left(e^{\xi_{Z1}s_i} - e^{\xi_{Z1}s_{i-1}}\right) + K_{2(x)}\left(e^{-\xi_{Z1}s_{i-1}} - e^{-\xi_{Z1}s_i}\right)\right], \\ \quad x_{12} < x \leq x_{23} \\ EAF_{(x_{23})} + \sqrt{\dfrac{EA\mu W_{Z4}}{\delta_{mob}}}\left[K_{1(x)}\left(e^{\xi_{Z4}s_i} - e^{\xi_{Z4}s_{i-1}}\right) + K_{2(x)}\left(e^{-\xi_{Z4}s_{i-1}} - e^{-\xi_{Z4}s_i}\right)\right], \\ \quad x_{23} \leq x < x_{34} \\ \mu W_{Z4} * (L - x), \quad x_{34} \leq x \leq L \end{cases} \tag{12}$$

See Appendix B for details on the mathematical development of equation (8) towards equation (12), based on the strategy adopted in .

With equation (12) the unknown values in Table 5 are derived and the full effective axial force profiles can be deduced via iteration on the position of x_{23}.

This solution scheme for the effective axial force profile for elastic-perfectly-plastic soils leads to the last step of the new calculation approach.

iv ΔS_S Revision

ΔS_S can be directly described as the summation of areas, as given by equation (13), and as schematically shown by Fig. 11.

$$\int_{SP_{SDown}}^{SP_{SUp}} (\Delta S_s)dx = -(|Area1| + |Area2| + |Area3| + |Area4|) \quad \textbf{(13)}$$

where each area represents the partial integral of effective axial force in terms of *x* coordinate accounting the physical boundaries as seen in Fig. 11.

9 WALKING RATE FOR ELASTIC-PERFECTLY-PLASTIC SOIL

Based on the above expressions, the walking rate for elastic-perfectly-plastic soils can be derived. Taking into account equation (5), the general modifications are:

$$WR_{EP} = -\frac{1}{EA}\left(\int_{SP_{SDown,EP}}^{SP_{SUp,EP}} (\Delta P)dx - \int_{SP_{SDown,EP}}^{SP_{SUp,EP}} (\Delta S_s)dx\right) \quad \textbf{(14)}$$

To validate this revised expression for WR_{EP}, a parametric finite element analyses study was conducted.

10 FINITE ELEMENT ANALYSES PARAMETRIC STUDY

The parametric study used a range of values for the following parameters:

- Pipeline length;
- Pipeline submerged weight;
- Friction factor;
- Route overall slope.

For these core properties three different values were attributed for each, resulting in 81 different combinations. The different values used are shown in Table 6.

Since the focus of this paper is the influence of axial mobilisation distance, eight different values of δ_{mob} were considered, in terms of pipeline steel outside diameter (OD), (0.03OD, 0.05OD, 0.06OD, 0.10OD, 0.15OD, 0.20OD, 0.33OD and 0.50OD), giving a total of 648 cases.

All 648 cases were modelled using the same finite element analyses solution. All respected the general behaviour for the pipeline walking phenomenon as expected (including the revised solutions).

Fig. 12 presents the finite element analyses results for X_{abEP} plotted against δ_{mob} for the 1° seabed slope while Fig. 13 compares X_{ab} achieved through finite element analyses and the equations proposed in this paper. Fig. 14, Fig. 15, Fig. 16 and Fig. 17 provide the same results for 2° and 3° seabed slopes, respectively.

In Fig. 13, Fig. 15 and Fig. 17 the results were plotted along with a line representing the equation (7) for each case. The finite element analyses results clearly validate equation (7).

At this stage, the results obtained for X_{ab} using the suggested formulation (equation (7)) and the finite element analyses' results were statistically analysed. For the 1° slope, the coefficient of determination, R^2, is equal to 0.986; whilst for 2° and 3°, R^2 is equal to 0.997 and 0.998, respectively. It is clear that the proposed methodology has a very strong accuracy. The authors also looked into the reason for the difference noticed in the 1° models, and it was found that some finite element models had an accidental limitation in terms of mesh. This generated a numerical noise that was reflected in the overall results. The noise can be eliminated through the use of a finer mesh in the models, thus retaining their applicability to any slope.

Fig. 18 shows the finite element model results for WR_{EP} plotted against δ_{mob} for the 1° seabed slope. Fig. 20 and Fig. 22 give the same results for 2° and 3° seabed slopes. Fig. 19, Fig. 21 and Fig. 23 present the comparison between finite element analyses and equation results.

Again, applying some statistics to the results shown by Fig. 19, Fig. 21 and Fig. 23, the coefficient of determination, R^2, was calculated to be 0.985 (for 1° slope), 0.997 (for 2° slope) and 0.999 (for 3° slope). These results confirm the level of accuracy of the findings of this paper and reinforce the applicability of the proposed methodology.

As it can be seen, the analytical expressions shown in sections 7, 8 and 9 agree closely with the finite element analyses results, as shown by the plots from Fig. 12 to Fig. 23.

Hence, for any straight pipeline resting on any sloping seabed with an elastic-perfectly-plastic soil we can conclude that the realistic walking rate might be written as:

$$WR_{EP} = WR_{RP} - ElasticCorr \tag{15}$$

Where the elastic correction, *ElasticCorr*, is equivalent to:

$$ElasticCorr = 2\left(\frac{Unload - Reload\ Area}{\Delta F}\right) \tag{16}$$

The *Unload-Reload Area* and the *ΔF* are exemplified in Fig. 3. Then, considering the single-spring elastic-perfectly-plastic approach, the entity *Elastic Correction* equals:

$$ElasticCorr = 2\left(\frac{2\mu W \cos\beta\, \delta_{mob}}{2\mu W \cos\beta}\right) = 2\delta_{mob} \tag{17}$$

Equation (17) also allows us to define the non-walking mobilisation distance, δ_{null}, to be:

$$\delta_{null} = \frac{WR_{RP}}{2} \tag{18}$$

11 CONCLUSIONS & FINAL REMARKS

This paper provides an analytical solution that solves pipeline walking problems for elastic-perfectly plastic (EP) pipe-soil response, benchmarked and validated against finite element analyses performed with an elastic-perfectly-plastic user-defined element. These revised solutions improve understanding of the parameters involved in elastic-perfectly-plastic soil behaviour for pipeline walking assessment. The paper resolves how the fundamental solution for rigid-plastic pipe-soil interaction requires expansion to allow for elasticity. It is shown that the "Stationary Points", which have zero movement during changes in the pipe temperature, do not coincide with the positions of maximum effective axial force (EAF). This is an important distinction compared to the rigid-plastic solution, in which the term "Virtual Anchor Point" is well-established as both the Stationary Point and the position of maximum effective axial force. Using the revised Stationary Points, the resulting mathematical proof shows the swept area within the effective axial force plot during a change in temperature remains a valid method to assess the pipeline expansion and contraction and therefore the pipeline walking. Relative to the rigid-plastic solution, the correction for elasticity is equivalent to the loss in area represented by the *Unload-Reload Area* inherent to the FxD soil curve.

Common solutions for pipeline walking, in which the soil is treated as rigid-plastic, invariably derive overestimates of walking action. Besides being unrealistic, a magnified walking rate can be onerous for projects, leading to additional effort and cost to mitigate pipeline walking.

Therefore, it is important to identify and apply realistic soil properties, and the solution in this paper allows the elastic-perfectly-plastic rather than rigid-plastic approach to be used.

The walking mechanism, explored in this paper, can now be assessed by a set of analytical expressions for walking evaluation, based on the general problem properties, such as, overall route slope, temperature variation and pipeline geometric data. These expressions were validated against a finite element analyses set.

12 ACKNOWLEDGMENT

This research forms part of the activities of the Centre for Offshore Foundation Systems (COFS), established under the Australian Research Council's Research Centres Program and currently supported as a node of the Australian Research Council Centre of Excellence for Geotechnical Science and Engineering. The authors acknowledge the support from The University of Western Australia and Shell.

NOMENCLATURE

A	steel area (cross section)
E	Steel Young's Modulus
EP	elastic-perfectly-plastic
EAF	effective axial force
FEA	finite element analysis
FEM	finite element model
FxD	force x displacement curve
HP	high pressure
HT	high temperature
KP	kilometre post
K_1	differential equation constant 1
K_2	differential equation constant 2
L	pipeline length
OD	overall pipe outside diameter
RP	rigid-plastic
R^2	coefficient of determination
s	distance to stationary point

SDown	shutdown phase
SUp	start-up phase
SP	stationary point
t	steel wall thickness
UEL	user element
VAS	virtual anchor section
W	pipeline submerged weight
W_{comp}	pipeline weight component
WR	walking rate
x	axial coordinate along pipe length
x_{12}	physical boundary between *Z1* and *Z2*
x_{23}	physical boundary between *Z2* and *Z3*
x_{34}	physical boundary between *Z3* and *Z4*
X_{ab}	distance between stationary points
Z1	route's zone 1
Z2	route's zone 2
Z3	route's zone 3
Z4	route's zone 4
α	steel thermal expansion coefficient

β	seabed slope angle
ΔS_S	effective axial force variation over Xab
ΔP	change in fully constrained force
ΔT	temperature variation
δ	general displacement
δ_{mob}	mobilisation distance
δ_{null}	non-walking mobilisation distance
δ_x	axial displacement
ε_{Mech}	mechanical strain
$\varepsilon_{Thermal}$	thermal strain
ε_{Total}	total strain
μ	axial friction coefficient
μW_{Z1}	resistant friction component in zone 1
μW_{Z4}	resistant friction component in zone 4
v	steel Poisson coefficient
ξ	differential equation exponential factor ξ

REFERENCES

[1] K. Tornes, B. A. Ose, J. Jury, and P. Thomson, “Axial Creeping of High Temperature Flowlines Caused by Soil Ratcheting,” in *Proceedings of the ETCE/OMAE2000 Joint Conference*, 2000.

[2] M. Carr, D. Bruton, and D. Leslie, “Lateral Buckling and Pipeline Walking, a Challenge for Hot Pipelines,” in *Proceedings of the Offshore Pipeline Technology Conference 2003*, 2003.

[3] D. Bruton, F. Sinclair, and M. Carr, “Lessons Learned From Observing Walking of Pipelines with Lateral Buckles, Including New Driving Mechanism and Updated Analysis Models,” in *Proceedings of the Offshore Technology Conference 2010*, 2010.

[4] D. White, M. E. Campbell, N. P. Boylan, and M. F. Bransby, “A new framework for axial pipe-soil interaction illustrated by shear box tests on carbonate soils,” in *Proceedings of the 2012 International Conference on Offshore Site Investigation and Geotechnics*, 2012.

[5] D. Bruton, D. J. White, M. Carr, and J. Cheuk, “Pipe-Soil Interaction During Lateral Buckling and Pipeline Walking - The SAFEBUCK JIP,” in *Proceedings of the Offshore Technology Conference 2008*, 2008.

[6] D. Carneiro and A. Castelo, “Walking Analyses of HP/HT Pipelines with Sliding End Structures Using Different FE Models,” in *Proceedings of the Rio Pipeline Conference & Exposition 2011*, 2011.

[7] D. Jayson, P. Delaporte, J.-P. Albert, M.-E. Prevost, D. Bruton, and F. Sinclair, “Greater Plutonio Project - Subsea Flowline Design and Performance,” in *Proceedings of the Offshore Flowline Technology Conference 2008*, 2008.

[8] M. Carr, F. Sinclair, and D. Bruton, “Pipeline Walking - Uderstanding the Field Layout Challenges, and Analytical Solutions Developed for the SAFEBUCK JIP,” in *Proceedings of the Offshore Technology Conference 2006*, 2006.

[9] D. J. White, S. Ganesan, M. Bolton, D. Bruton, J.-C. Ballard, and T. Langford, “SAFEBUCK JIP - Observations of Axial Pipe-Soil Interaction from Testing on Soft Natural Clays,” in *Proceedings of the Offshore Technology Conference 2011*, 2011.

[10] A. J. Hill, D. White, D. Bruton, T. Langford, V. Meyer, R. Jewell, and J.-C. Ballard, “A New Framework for Axial Pipe-Soil Resistance, Illustrated by a Range of Marine Clay Datasets,” in *Proceedings of the 2012 International Conference on Offshore Site Investigation and Geotechniques*, 2012.

[11] R. E. Hobbs, “In-Service Buckling of Heated Pipelines,” *ASCE Journal of Transportation Engineering*, vol. 110, pp. 175–189, 1984.

[12] M. Randolph, “A Theoretical Study of the Performance of Piles,” PhD Thesis, University of Cambridge, 1977.

Figure Captions List

Fig. 1	EAF diagrams for SUp and SDown
Fig. 2	δ_x diagrams for SUp and SDown phases
Fig. 3	RP & EP soil responses
Fig. 4	Finite element model sketch
Fig. 5	EAF plot (Zoom)
Fig. 6	δ_x plot for Stiff Fit (Zoom)
Fig. 7	δ_x plot for Soft Fit (Zoom)
Fig. 8	x Coordinate for the SPs
Fig. 9	X_{abEP} results against δ_{mob}
Fig. 10	Schematic plot accounting physical boundaries
Fig. 11	Schematic EAF plot with the partial areas highlight
Fig. 12	X_{abEP} results for 1° slope
Fig. 13	X_{abEP} results – Numerical (FEA) & Calculated (Equations) – for 1° slope
Fig. 14	X_{abEP} results for 2° slope
Fig. 15	X_{abEP} results – Numerical (FEA) & Calculated (Equations) – for 2° slope
Fig. 16	X_{abEP} results for 3° slope
Fig. 17	X_{abEP} results – Numerical (FEA) & Calculated (Equations) – for 3° slope
Fig. 18	WR_{EP} results for 1° slope

Table Caption List

FIGURES

Fig. 1 EAF diagrams for SUp and SDown phases

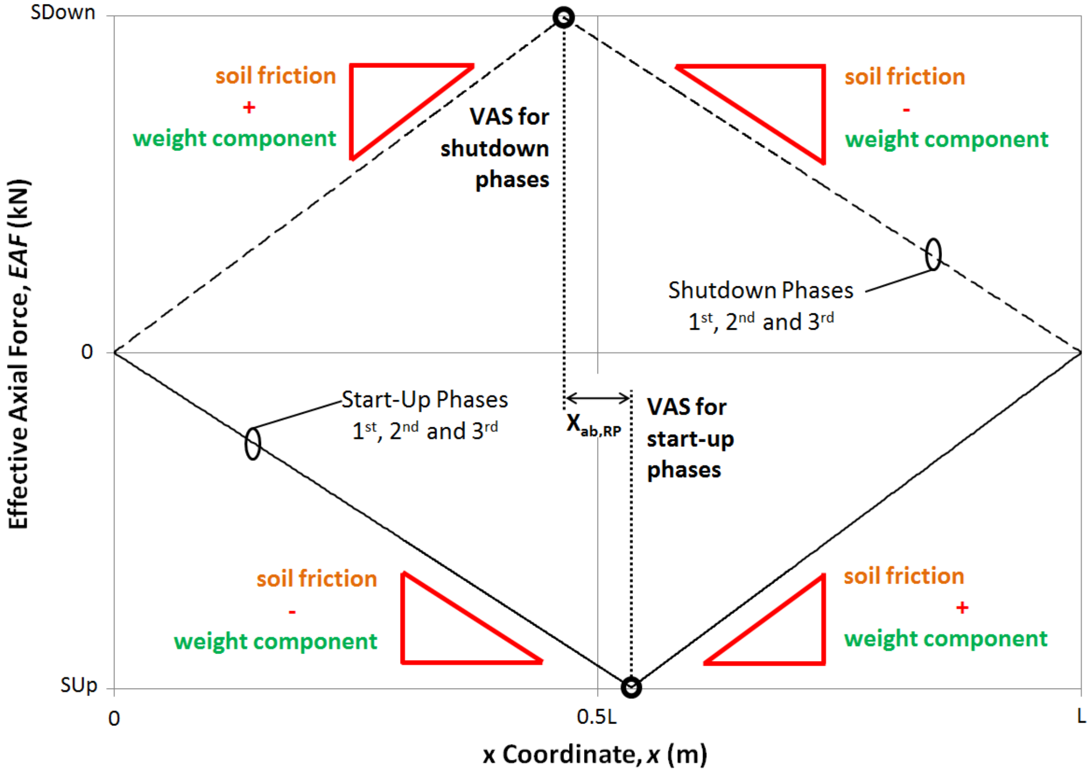

Fig. 2 δ_x diagrams for SUp and SDown phases

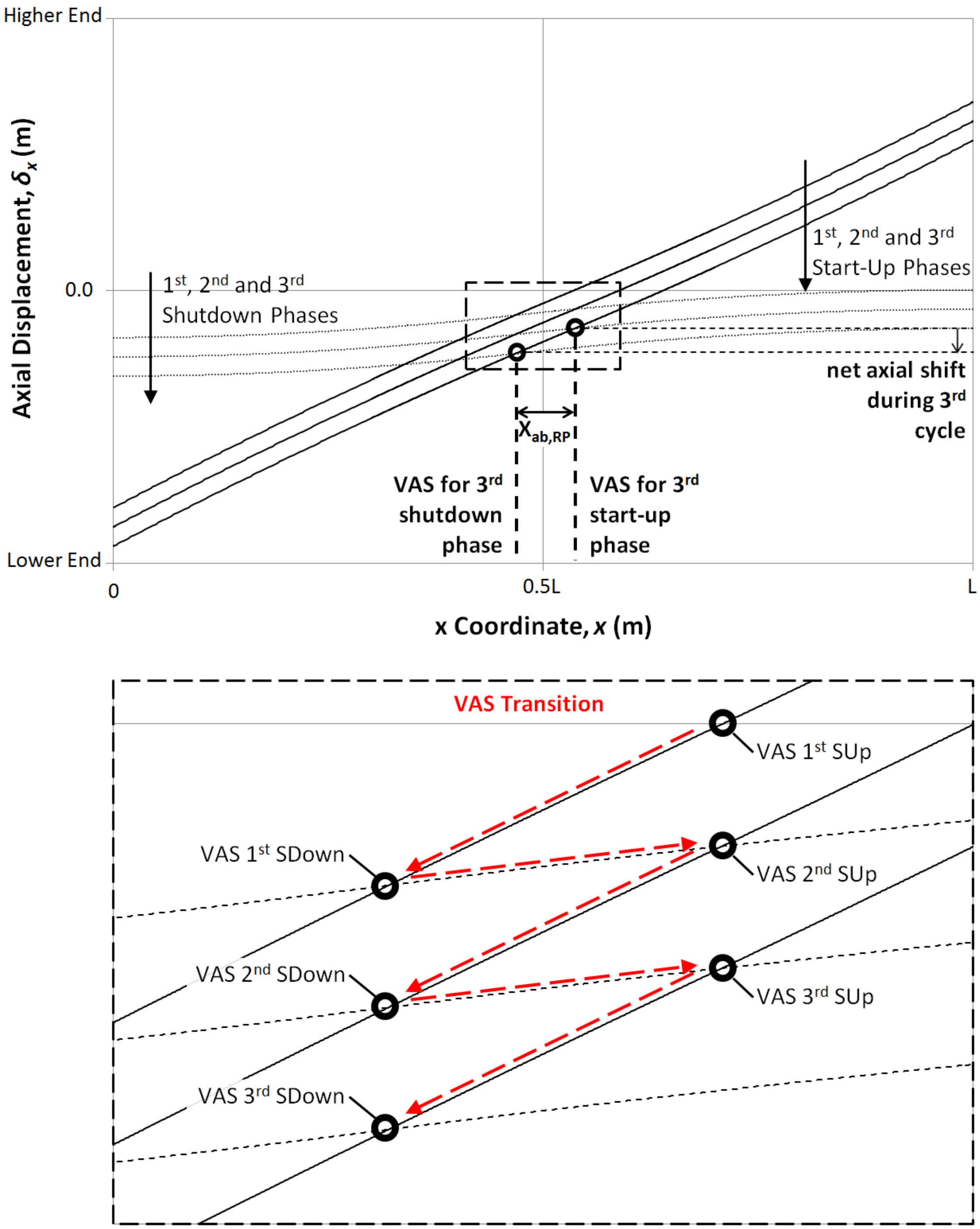

Fig. 3 RP & EP soil responses

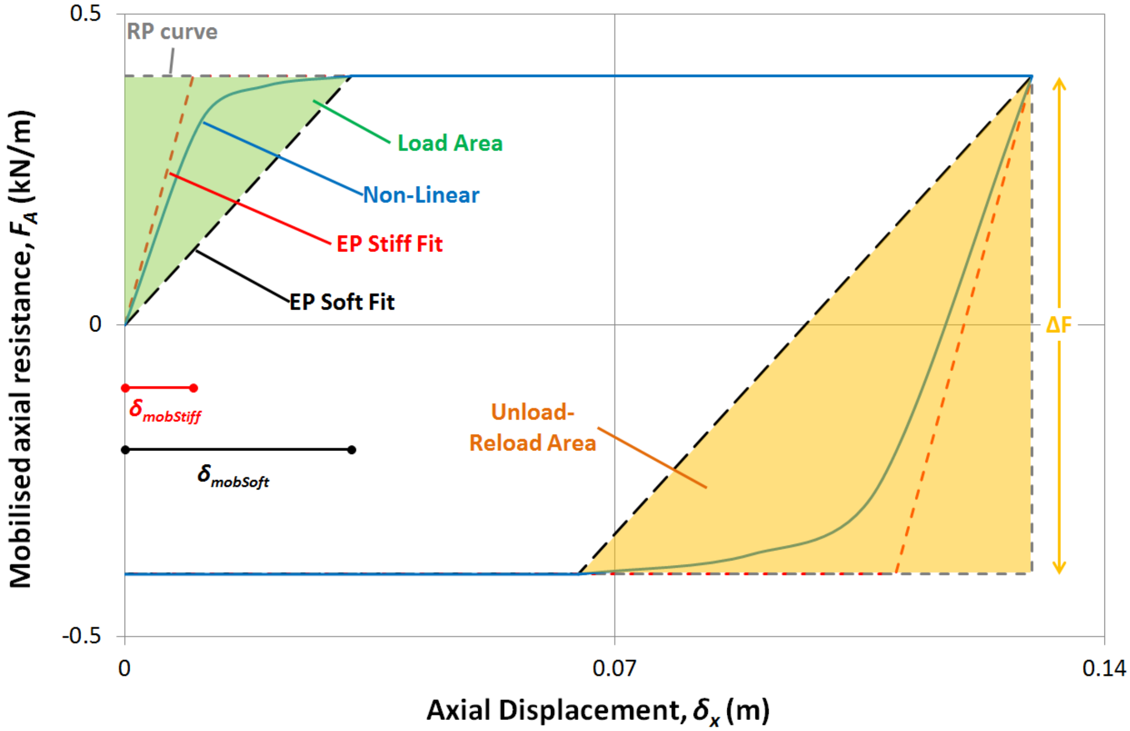

423 **Fig. 4 Finite element model sketch**

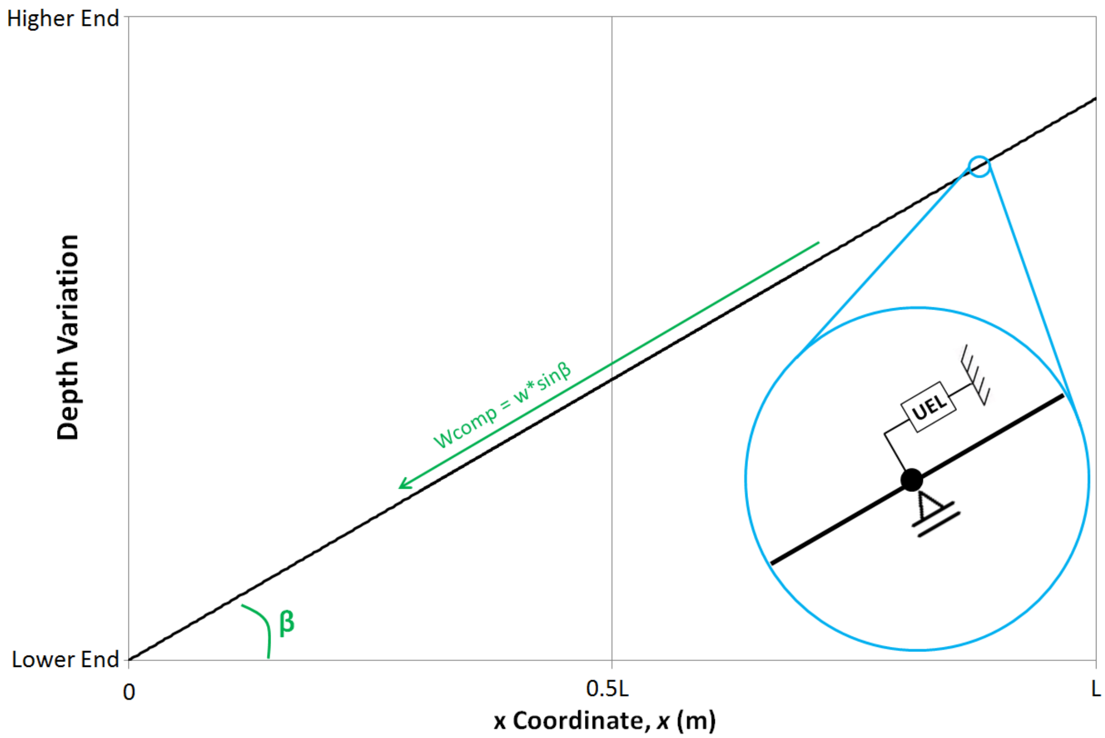

424

425

Fig. 5 EAF plot (Zoom)

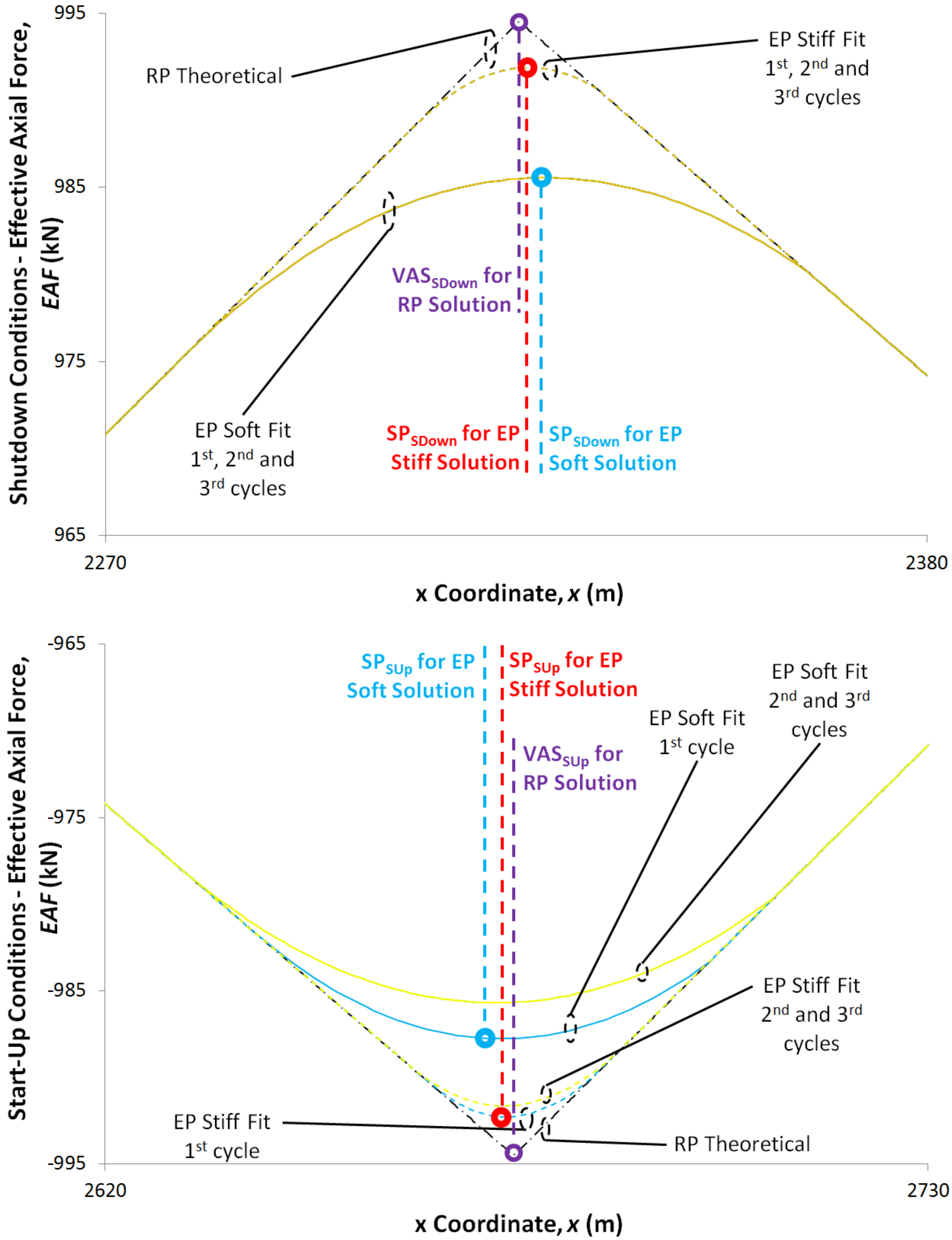

Fig. 6 δ_x plot for Stiff Fit (Zoom)

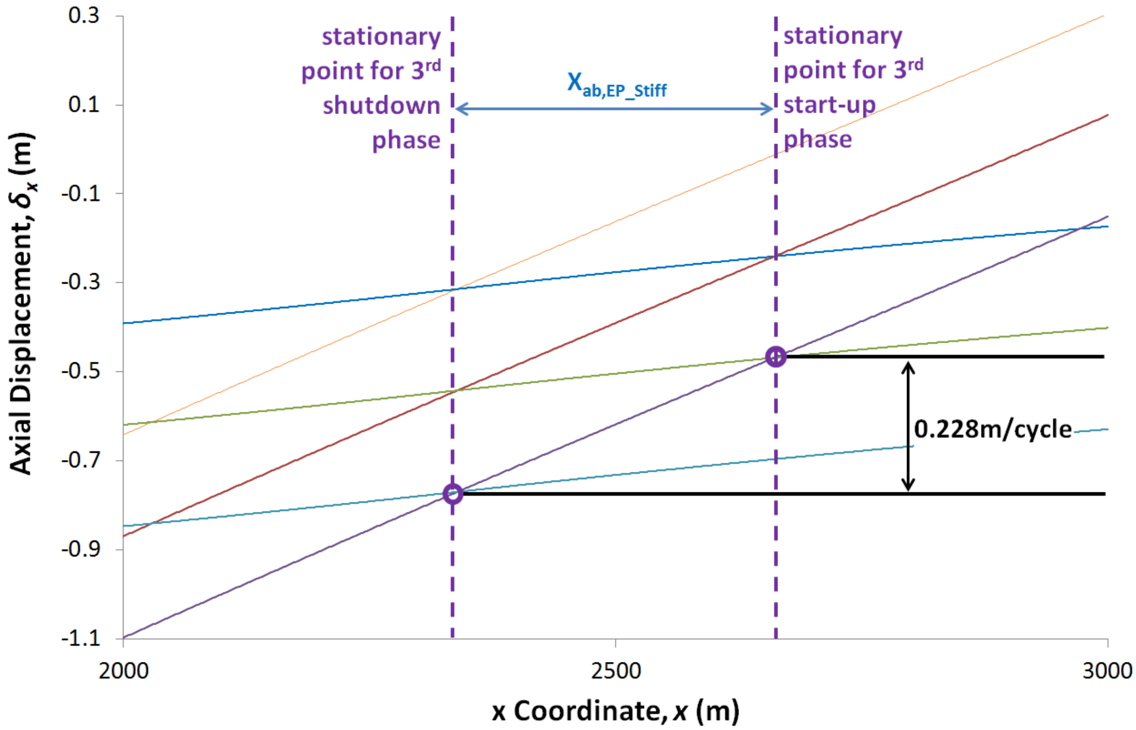

Fig. 7 δ_x plot for Soft Fit (Zoom)

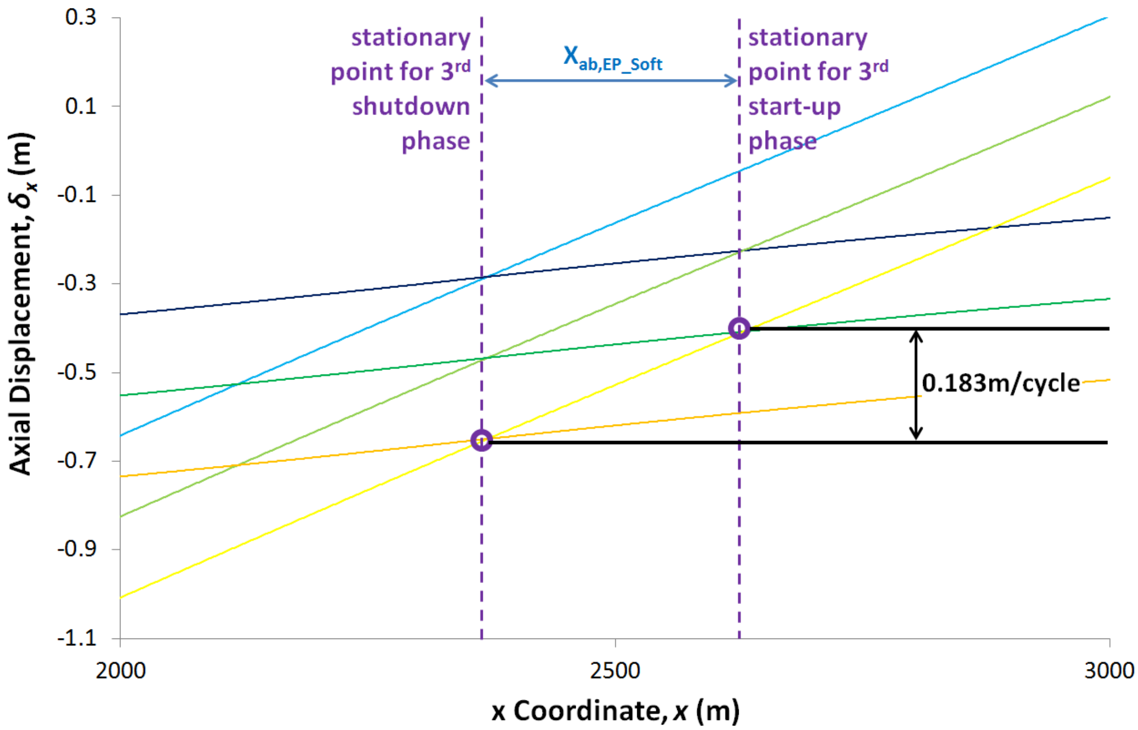

439 **Fig. 8 x Coordinate for the SPs**

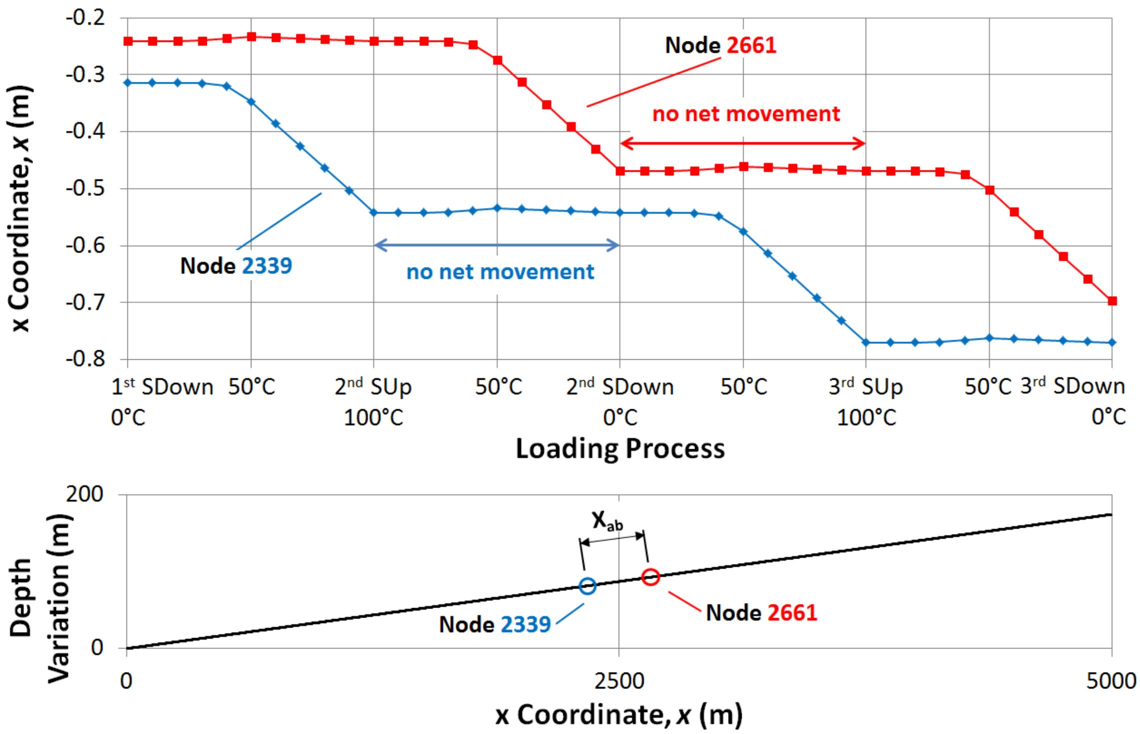

440

441

442

443 **Fig. 9 X_{abEP} results against δ_{mob}**

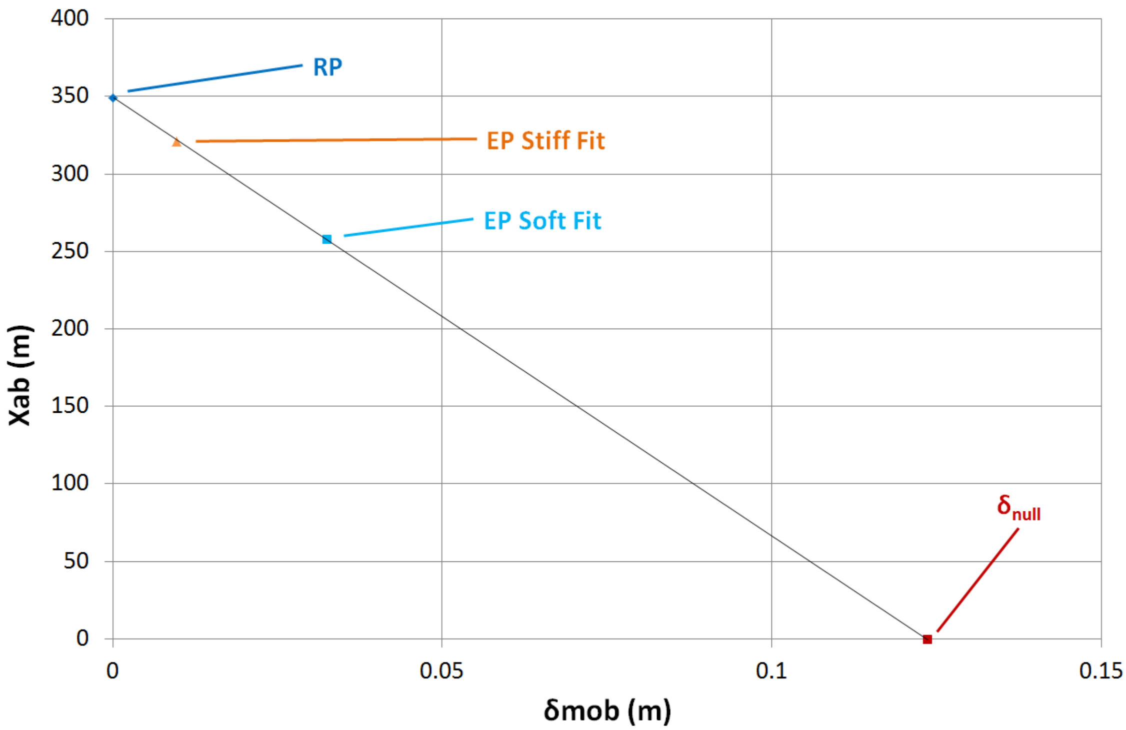

444
445

446

Fig. 10 Schematic plot accounting physical boundaries

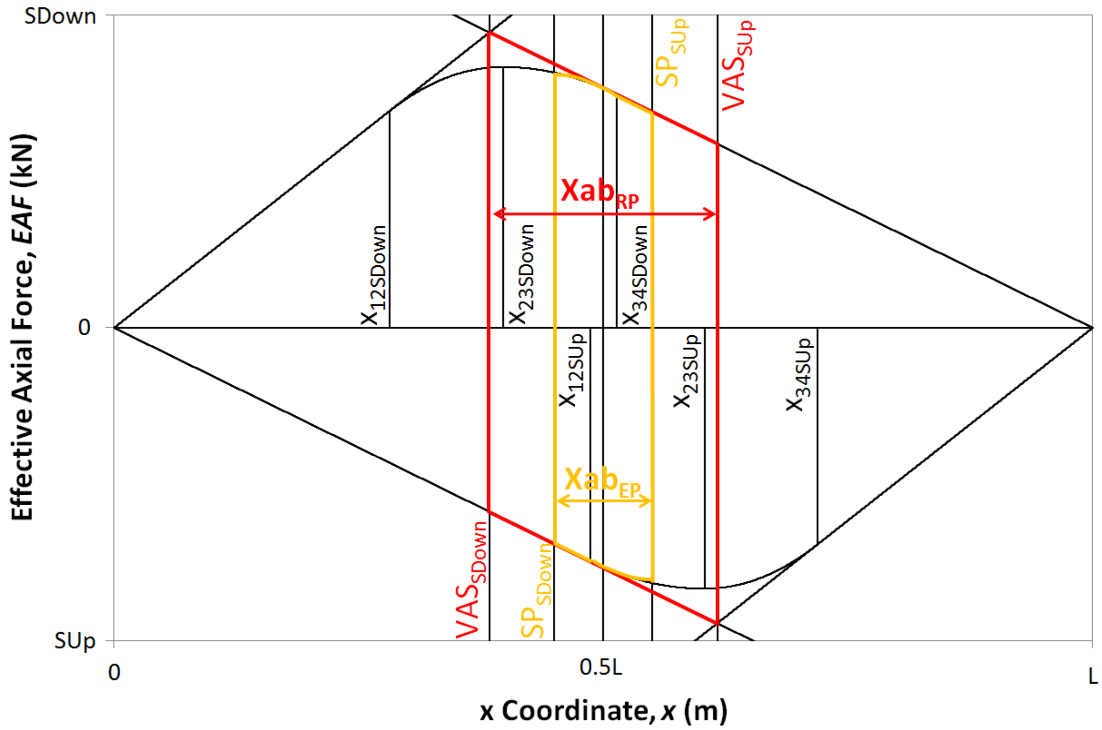

Fig. 11 Schematic EAF plot with the partial areas highlight

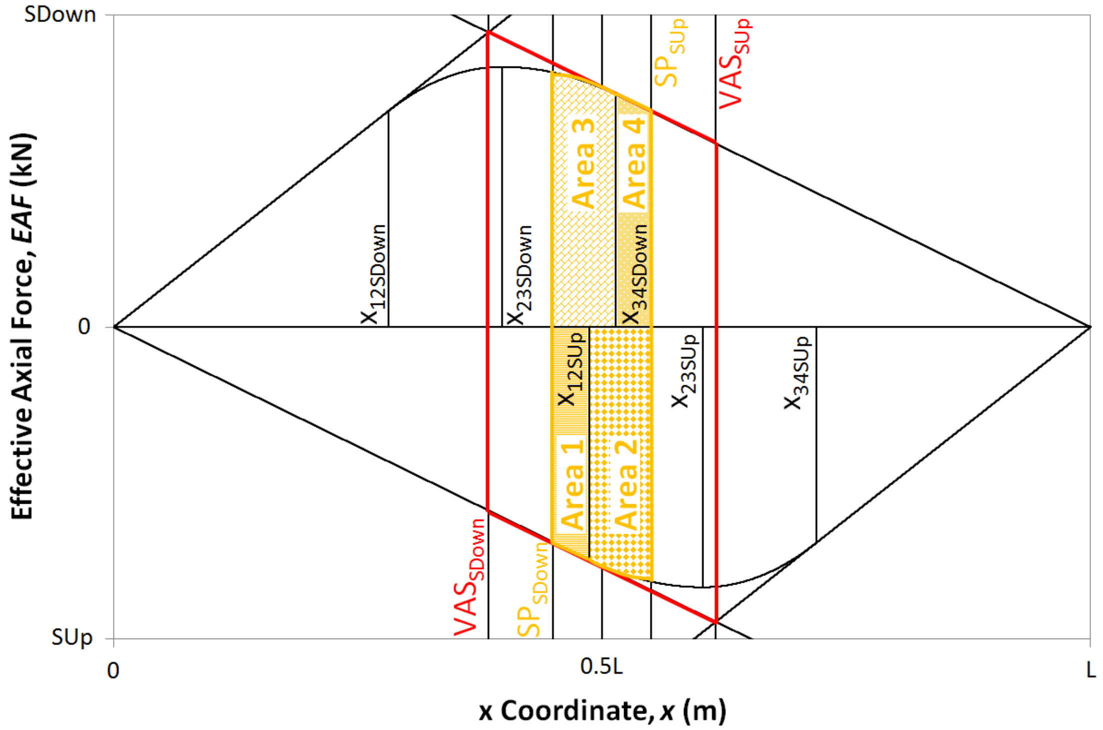

Fig. 12 X_{abEP} results for 1° slope

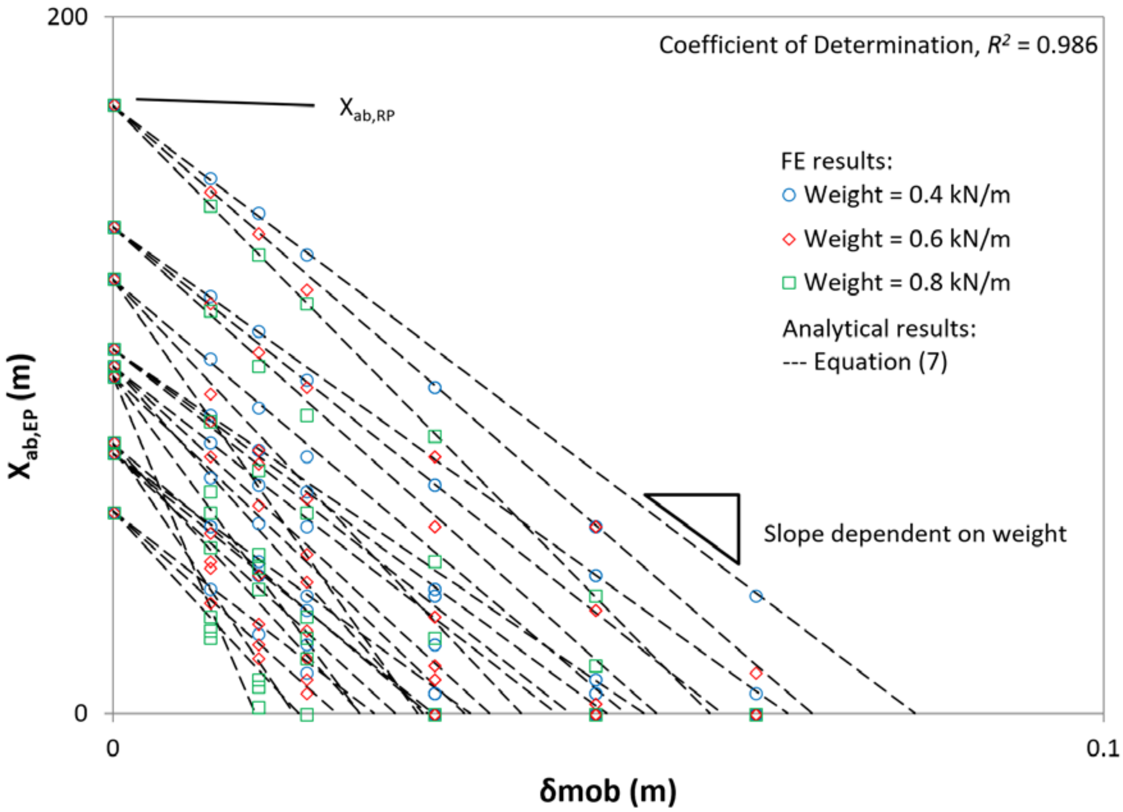

Fig. 13 X_{abEP} results – Numerical (FEA) & Calculated (Equations) – for 1° slope

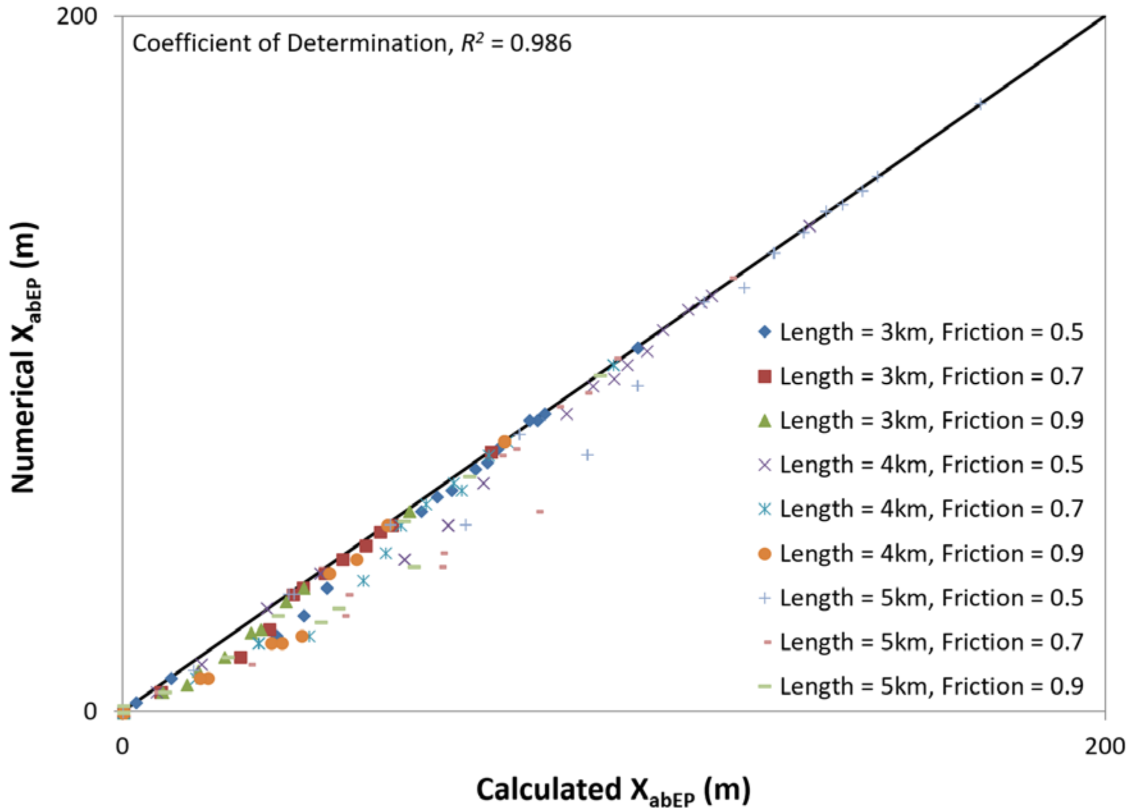

Fig. 14 X_{abEP} results for 2° slope

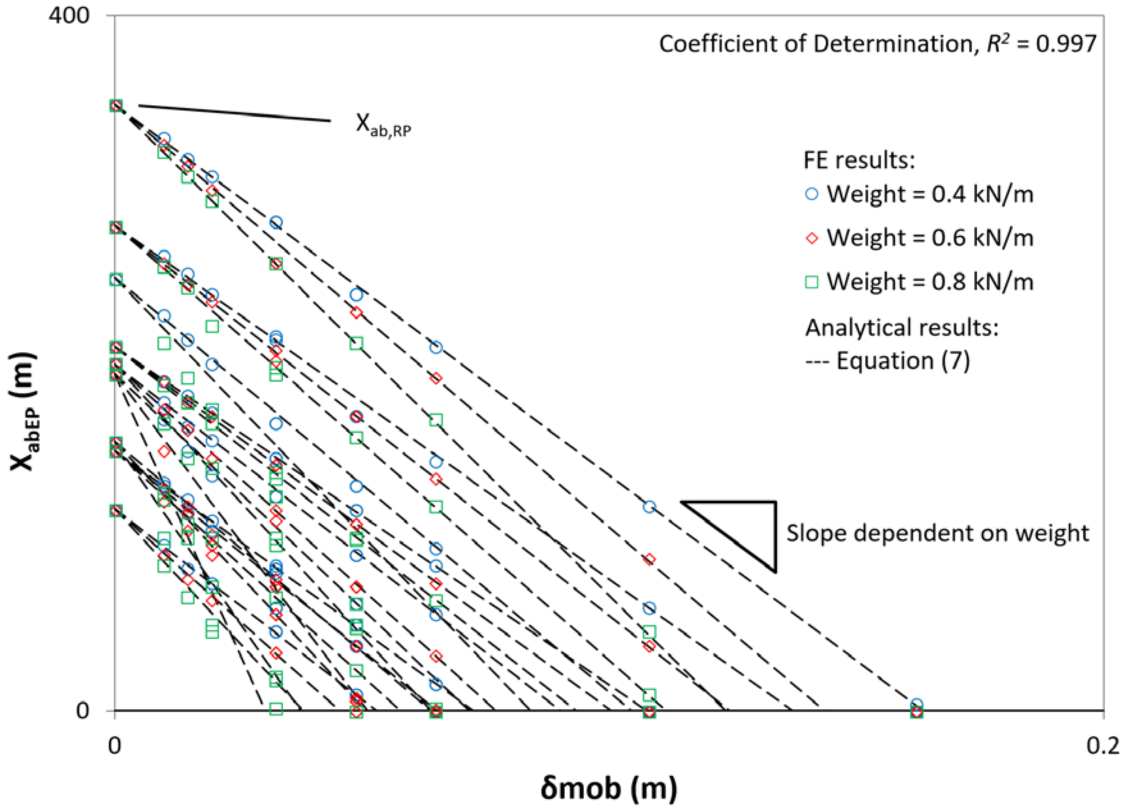

Fig. 15 X_{abEP} results – Numerical (FEA) & Calculated (Equations) – for 2° slope

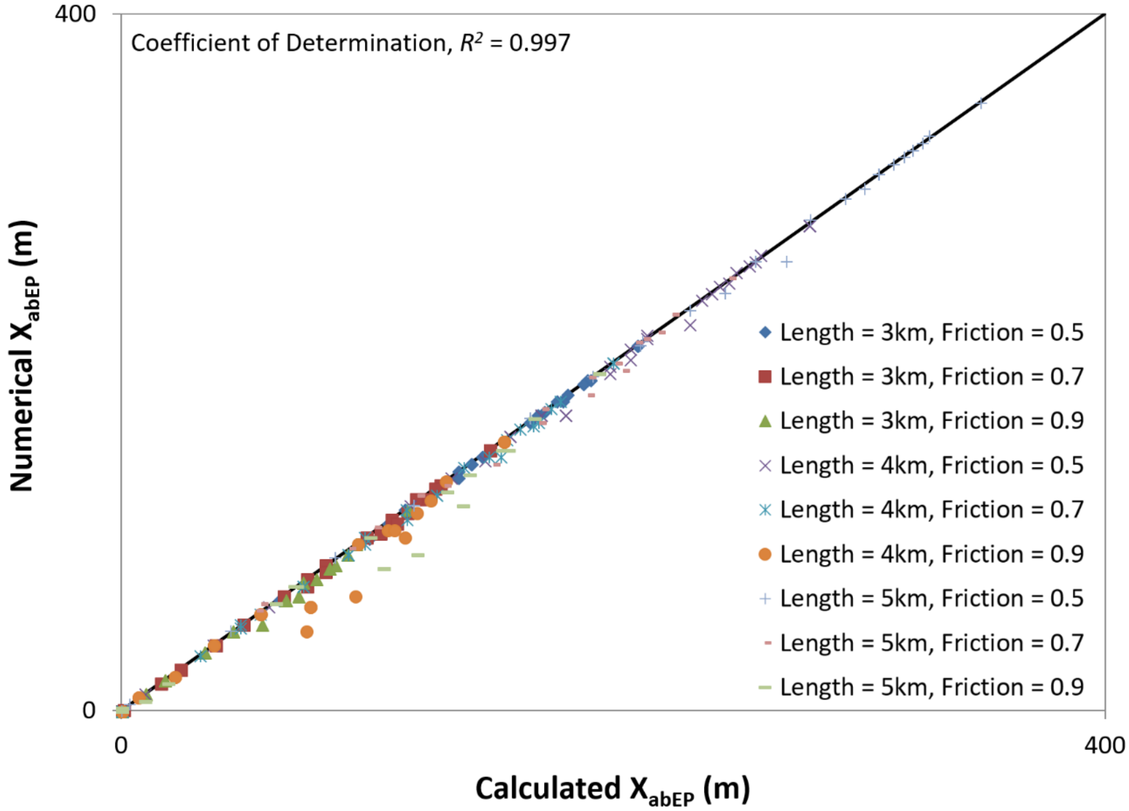

469 **Fig. 16 X_{abEP} results for 3° slope**

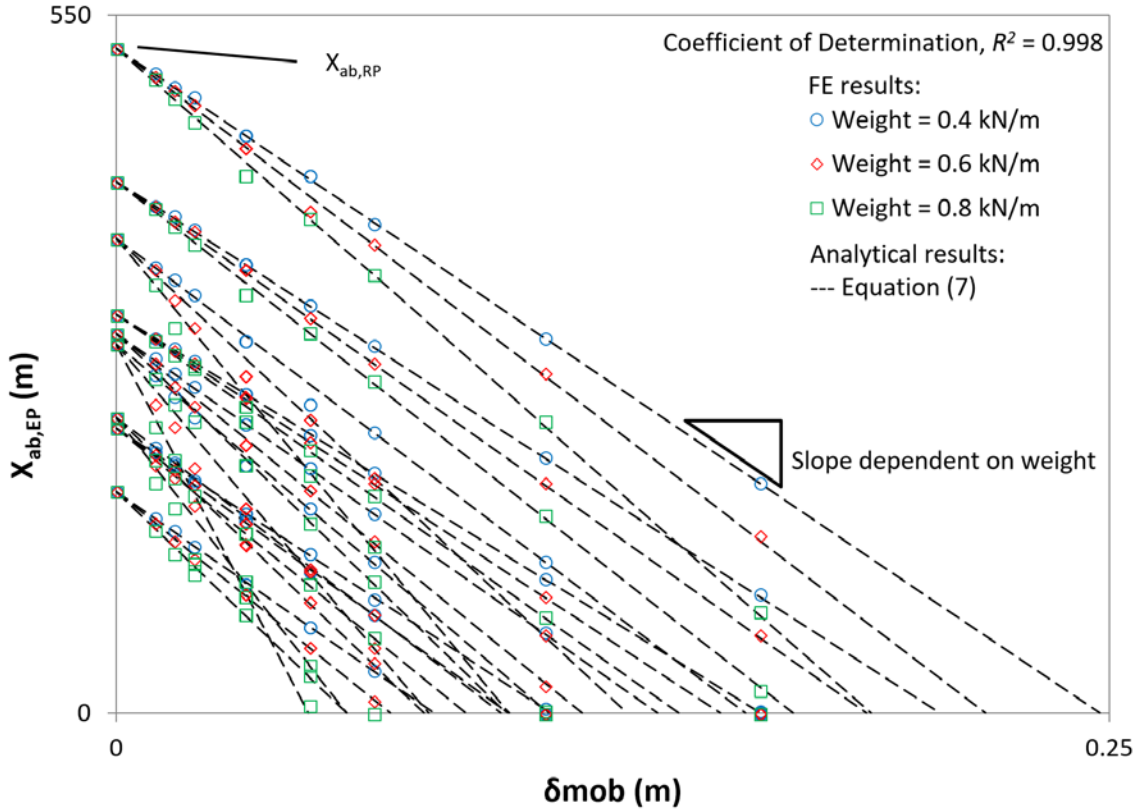

470
471

472

Fig. 17 X_{abEP} results – Numerical (FEA) & Calculated (Equations) – for 3° slope

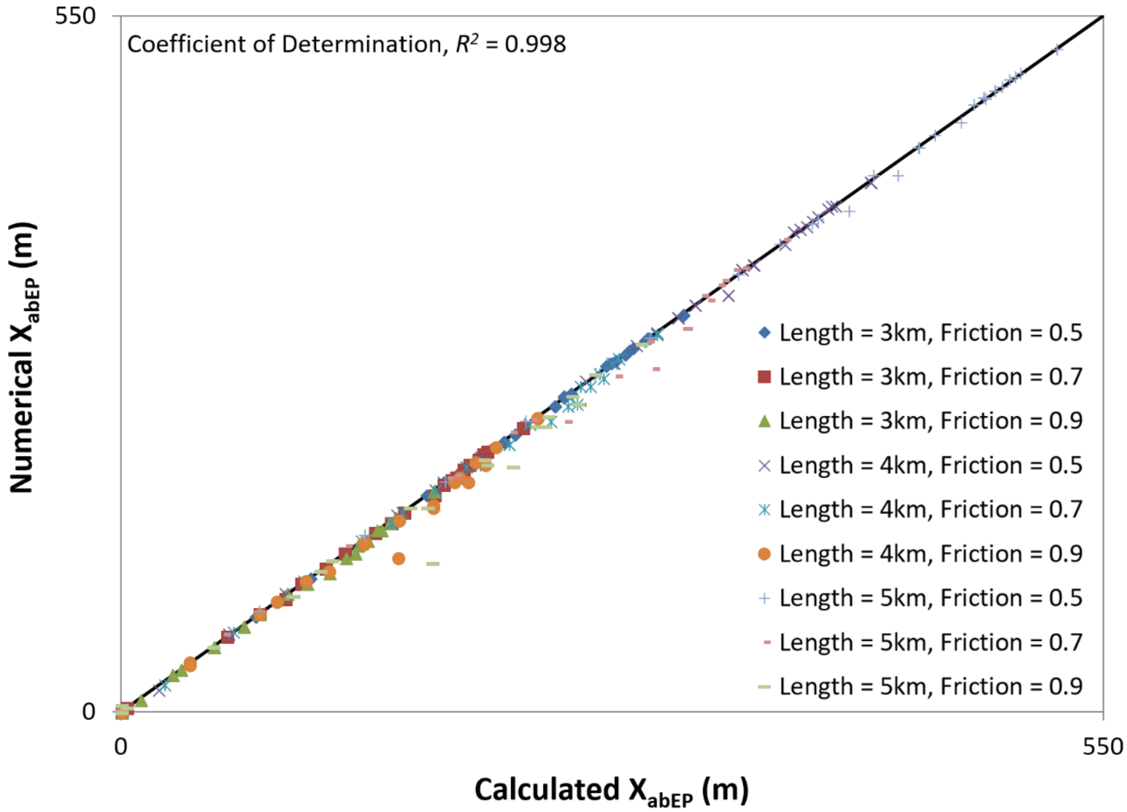

Fig. 18 *WR_{EP}* results for 1° slope

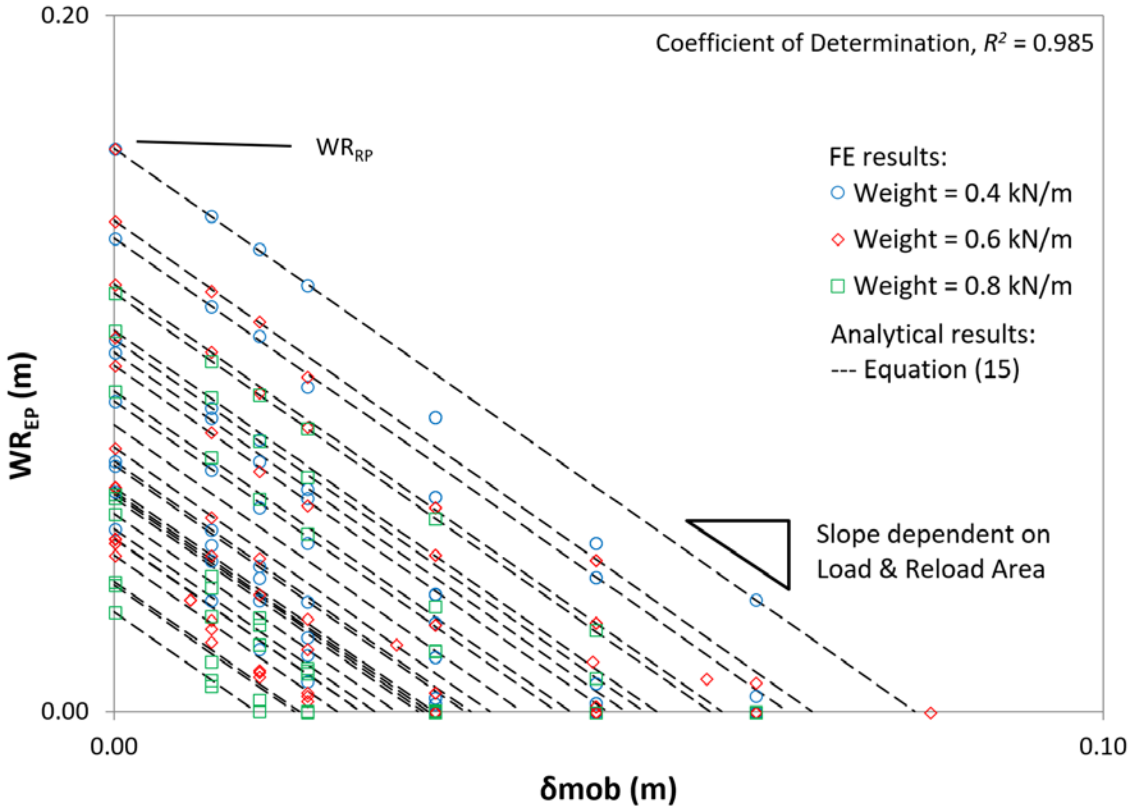

Fig. 19 *WR_{EP}* results – Numerical (FEA) & Calculated (Equations) – for 1° slope

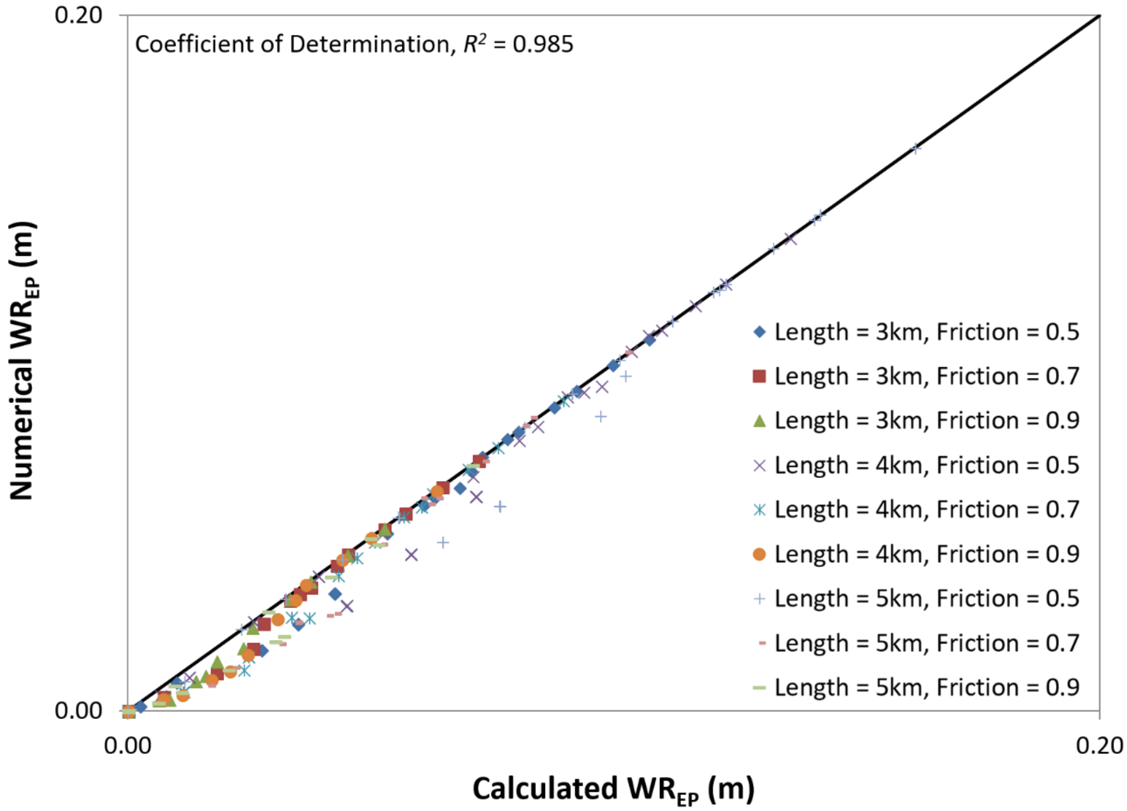

Fig. 20 WR_{EP} results for 2° slope

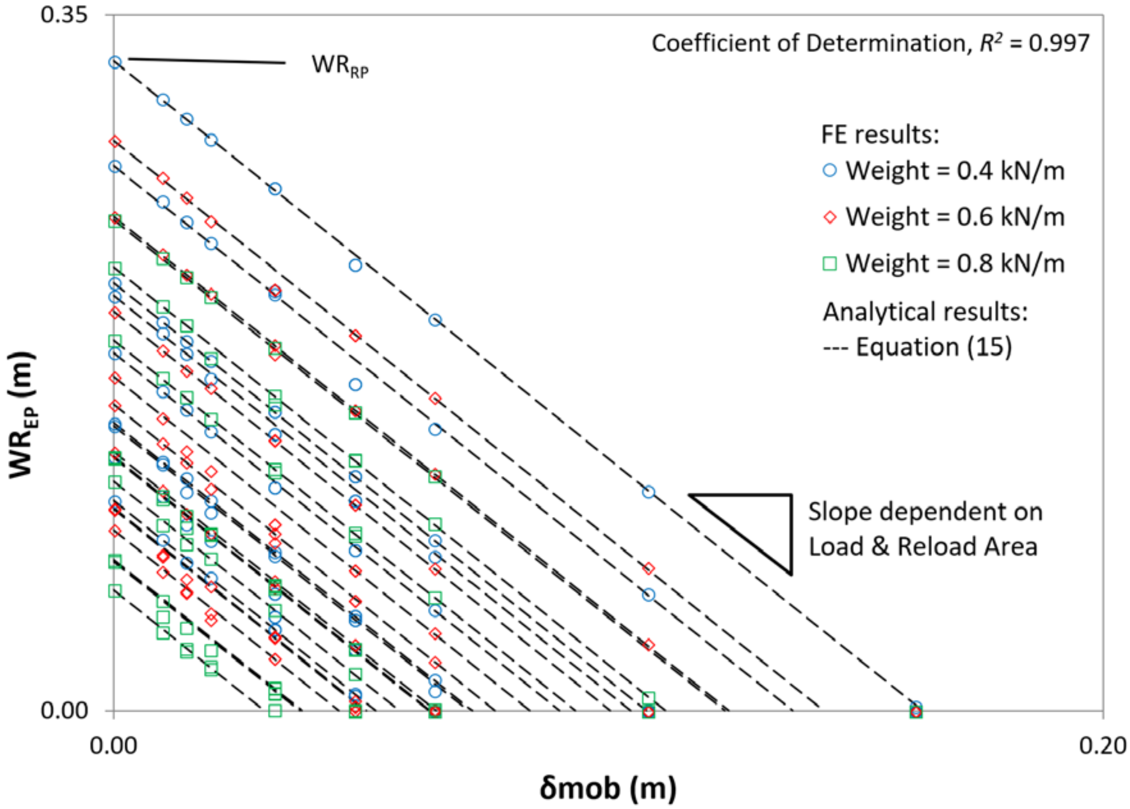

Fig. 21 *WR_{EP}* results – Numerical (FEA) & Calculated (Equations) – for 2° slope

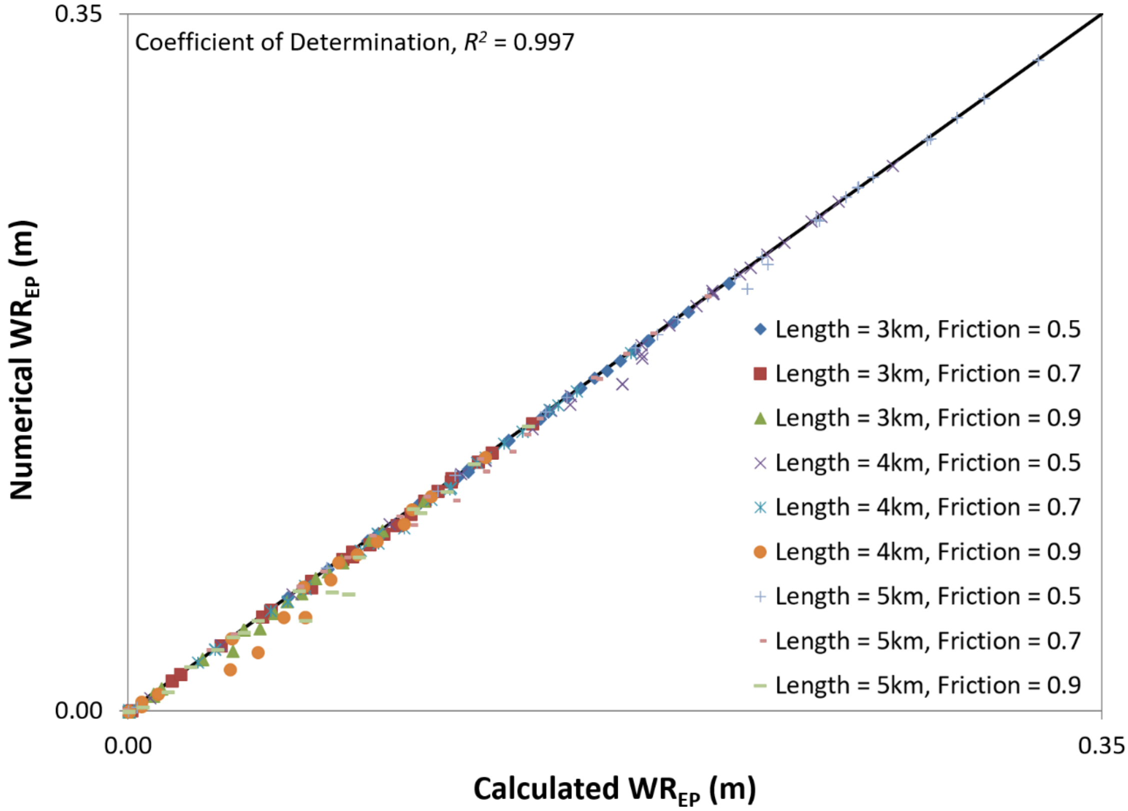

493 **Fig. 22 *WR_{EP}* results for 3° slope**

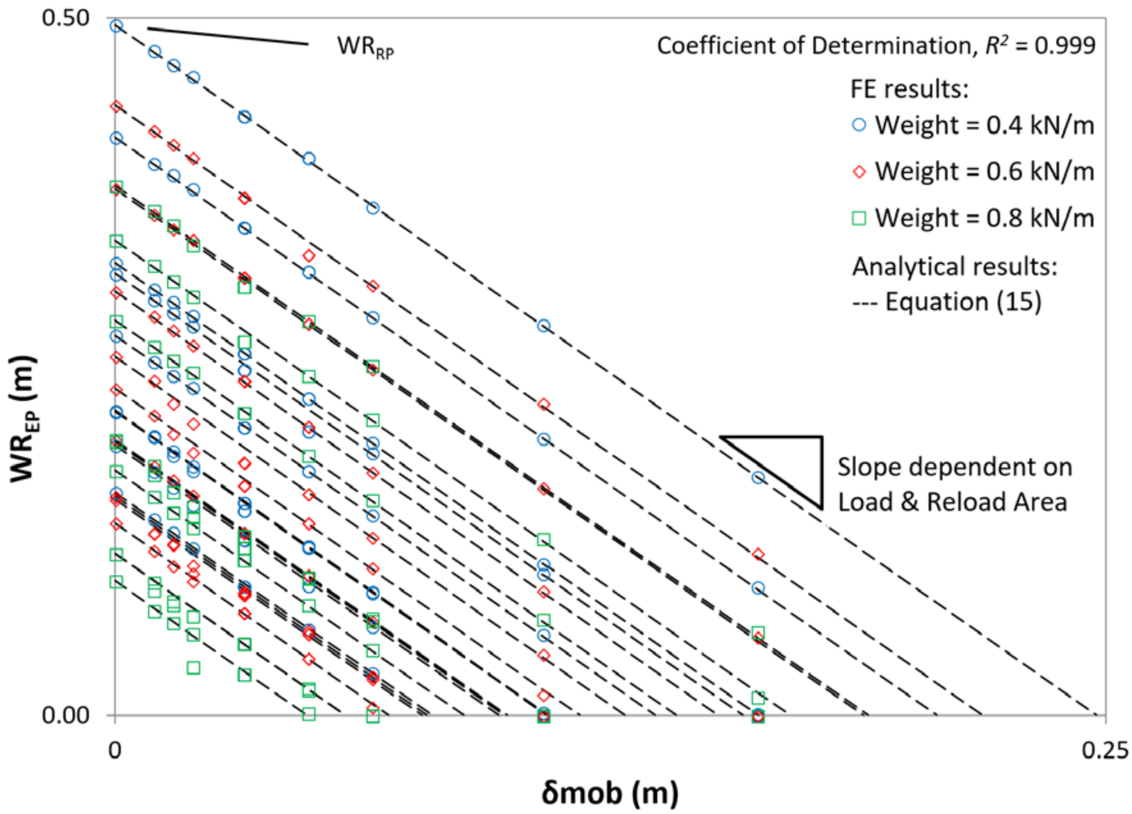

494
495

496

Fig. 23 *WR_{EP}* results – Numerical (FEA) & Calculated (Equations) – for 3° slope

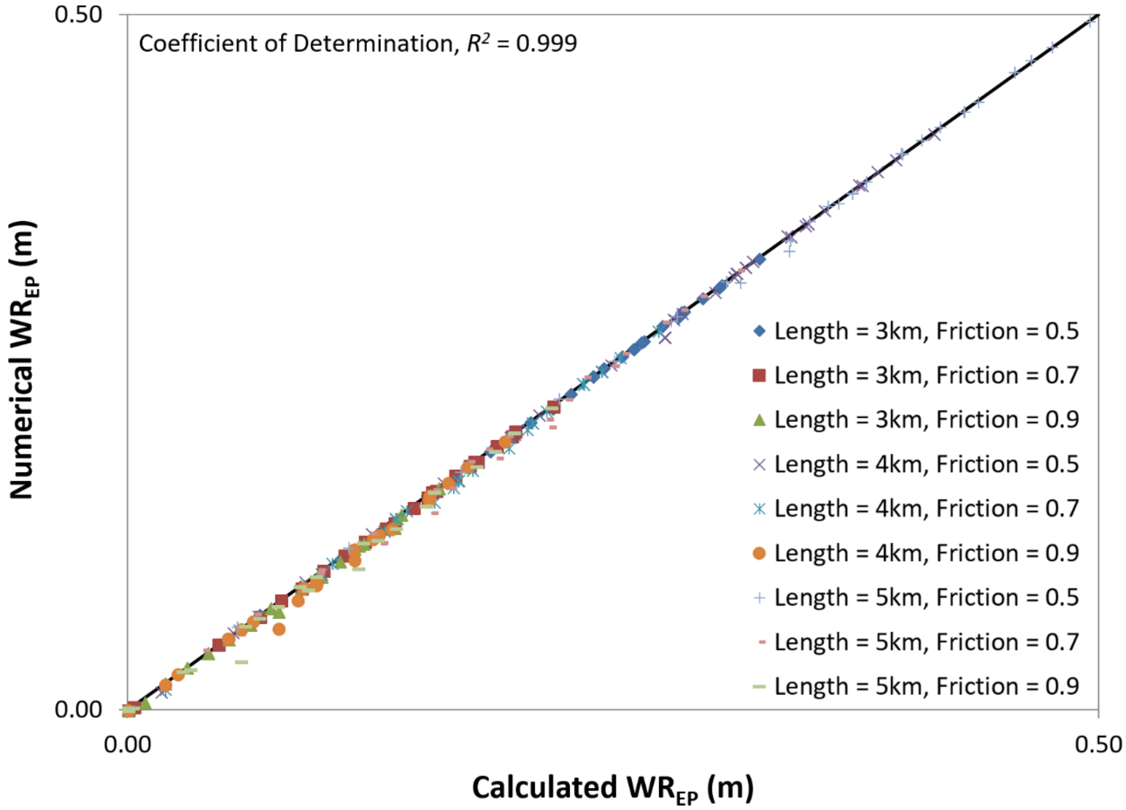

TABLES

Table 1 Preliminary example properties

Parameter	Value
Steel Outside Diameter, *OD*	0.3239m
Steel Wall Thickness, *t*	0.0206m
Length, *L*	5000m
Seabed Slope, *β*	2.0°
Temperature Variation, *ΔT*	100°C
Pipe Submerged Weight, *W*	0.8kN/m
Friction factor, *μ*	0.5
Steel Young's Modulus, *E*	2.07×10^{11}Pa
Steel Poisson Coefficient, *v*	0.3
Steel Thermal Expansion Coefficient, *α*	1.165×10^{-5}°C^{-1}
Mobilisation Distance for Stiff Fit, $\delta_{mobStiff}$	0.03OD
Mobilisation Distance for Soft Fit, $\delta_{mobSoft}$	0.10OD

505 **Table 2 RP analytical results**

Parameter	Value
$X_{ab,RP}$	349.208m
$\Delta S_{S,RP}$	-1859.184kN
WR_{RP}	0.247m/cycle

506

507

Table 3 EP FEA results

Parameter	Source	Value
$X_{ab,RP}$	EAF & δ_x - Fig. 1, Fig. 2 and equation (1)	349m
X_{ab,EP_Stiff}	EAF - Fig. 5	347m
X_{ab,EP_Stiff}	δ_x - Fig. 6	321m
X_{ab,EP_Soft}	EAF - Fig. 5	343m
X_{ab,EP_Soft}	δ_x - Fig. 7	258m

Table 4 Pipeline zoning

Zone	Initial KP	Final KP
Z1	0	x_{12}
Z2	x_{12}	x_{23}
Z3	x_{23}	x_{34}
Z4	x_{34}	L

Table 5 EAF boundary conditions

x coordinate	EAF	$\frac{dEAF}{dx}$
0	0	$W(\mu\cos\beta+\sin\beta)$
x_{12}	$x_{12}[W(\mu\cos\beta+\sin\beta)]$	$W(\mu\cos\beta+\sin\beta)$
x_{23}	?	0
x_{34}	$x_{34}[W(\mu\cos\beta-\sin\beta)]$	$W(\mu\cos\beta-\sin\beta)$
L	0	$W(\mu\cos\beta-\sin\beta)$

Table 6 FEA parametric variables

Parameter	Value A	Value B	Value C
Length (m)	3000	4000	5000
Weight (kN/m)	0.4	0.6	0.8
Friction (-)	0.5	0.7	0.9
Slope (°)	1	2	3

APPENDIX A

In this appendix some auxiliary equations are listed, in order to keep the main text concise, focused and direct.

From equation (19) to (22) the authors presented some secondary equations related to item 4.

$$X_{ab,RP} = \left(VAS_{SUp} - VAS_{SDown}\right) \quad \textbf{(19)}$$

$$VAS_{SUp,RP} = \left(\frac{L + X_{ab,RP}}{2}\right) \quad \textbf{(20)}$$

$$VAS_{SDown,RP} = \left(\frac{L - X_{ab,RP}}{2}\right) \quad \textbf{(21)}$$

$$\Delta P = -(p_2 - p_1)A_i(1 - 2\nu) - EA_s\alpha(T_2 - T_1) \quad \textbf{(22)}$$

APPENDIX B

Appendix B gives more details on the pile/ pipe equivalence as stated by item 8 accordingly with [12].

a Basic Mechanics Revision

$$\varepsilon_{Mech} = \frac{F}{EA} \quad \textbf{(23)}$$

$$\varepsilon_{Total} = \frac{d\delta}{dx} \quad \textbf{(24)}$$

$$(\varepsilon_{Mechanical} + \varepsilon_{Thermal}) = \frac{d\delta}{dx} \quad \textbf{(25)}$$

$$\frac{d^2\delta}{dx^2} = \frac{1}{EA}\frac{dF}{dx} + \alpha\Delta T \quad \textbf{(26)}$$

b Longitudinal Coordinate

The longitudinal coordinate, in equation (8) referred to as *x*, was substituted by the section distance, *s*, as expressed by equation (27); where *x* is the absolute KP value of the section in question and x_{23} is the boundary KP value for the case assessed, as previously explained.

$$s = |x - x_{23}| \quad \textbf{(27)}$$

c Factor ξ

To get this factor expression, put all zones apart and do the calculations only for *Z1*, the other zones will be later checked to prove whether this result is valid or not.

Hence, putting together equations (8) and (11) we can achieve the following system of equations:

$$\begin{cases} \delta = K_1 e^{\xi_{Z1}*s} + K_2 e^{-\xi_{Z1}*s} \\ \dfrac{dF}{dx} = \left(\dfrac{\mu W_{Z1}}{\delta_{mob}}\right)\delta \\ \dfrac{dF}{dx} = EA\left(K_1 {\xi_{Z1}}^2 e^{\xi_{Z1}*s} + K_2 {\xi_{Z1}}^2 e^{-\xi_{Z1}*s}\right) \end{cases} \quad \textbf{(28)}$$

And from this system of equations, we can extract:

$$\xi_{Z1} = \sqrt{\left(\frac{\mu W_{Z1}}{EA\delta_{mob}}\right)} \quad \textbf{(29)}$$

From the final shape of its expression, we can conclude that for zones *Z1* and *Z2*, ξ has the same value; and, this is also valid for zones *Z3* and *Z4*. Then, there are actually only two values for factor ξ, ξ_{Z1} and ξ_{Z4} applicable for zones *Z1* & *Z2* and *Z3* & *Z4*, respectively.

d Constants K_1 and K_2

Analogously to Randolph's equations (4.27) and (4.28), we needed to define a pair of equations suited to the present problem, to be considered at a single position of the pipe.

Equation (30) is related to x_{23} displacement, while equation (31) is related to its third derivative through the second derivative of force.

$$\delta_{(x23)} = \left(K_1 e^{\xi_{Z1}*s} + K_2 e^{-\xi_{Z1}*s}\right)_{(x_{23})} \quad \textbf{(30)}$$

$$\frac{d^2F}{dx^2}_{(x23)} = EA\xi_{Z1}{}^3\left(K_1 e^{\xi_{Z1}*s} - K_2 e^{-\xi_{Z1}*s}\right)_{(x_{23})} \quad \textbf{(31)}$$

For x_{23}, we can simplify the exponential portions as equal to 1, because the *s* exponent will assume the value of 0 (zero). The notation *Z1* was used in this item, but it could be used *Z4*, as well, because x_{23} is the limit between the different zones. Therefore, because of point x_{23}'s nature, equation (30) and equation (31) might be rewritten with *Z4* indexes. This also means that the force acting at x_{23} might be dependent on *Z1* or *Z4* and they must provide the same force result.

Tackling first equation (30), we will have – analogously to Randolph's equation (4.28) – using the δ_x boundary conditions (item 8i):

$$\begin{gathered}\delta_{(x_{23})} = 0 \\ \left(K_1 e^{\xi_{Z1} * s} + K_2 e^{-\xi_{Z1} * s}\right)_{(x_{23})} = 0 \\ (K_1 + K_2)_{(x_{23})} = 0\end{gathered} \tag{32}$$

Before handling equation (31), we need to take a step back and look at the following relations:

$$\begin{gathered}\frac{d^2F}{dx^2} = \frac{d\,\dfrac{dF}{dx}}{dx} \\ \frac{d^2F}{dx^2} = \frac{d\left(\dfrac{\mu W_{Z1}}{\delta_{mob}}\right)\delta}{dx} \\ \frac{d^2F}{dx^2} = \left(\frac{\mu W_{Z1}}{\delta_{mob}}\right)\frac{d\delta}{dx} \\ \frac{d^2F}{dx^2} = \left(\frac{\mu W_{Z1}}{\delta_{mob}}\right)\varepsilon_{Total} \\ \frac{d^2F}{dx^2} = \left(\frac{\mu W_{Z1}}{\delta_{mob}}\right)(\varepsilon_{Mechanical} + \varepsilon_{Thermal}) \\ \frac{d^2F}{dx^2} = \left(\frac{\mu W_{Z1}}{\delta_{mob}}\right)\left(\frac{F}{EA} + \alpha\Delta T\right) = \frac{\mu W_{Z1}}{EA\delta_{mob}} * F + \frac{\mu W_{Z1}\alpha\Delta T}{\delta_{mob}}\end{gathered} \tag{33}$$

Then, equating expression (31) with the final product of expression (33) we'll have:

$$(K_1 - K_2)_{(x_{23})} = \left(\frac{\mu W_{Z1}}{{\xi_{Z1}}^3 EA^2\delta_{mob}} * F + \frac{\mu W_{Z1}\alpha\Delta T}{{\xi_{Z1}}^3 EA\delta_{mob}}\right)_{(x_{23})} \tag{34}$$

Working with equations (32) and (33) as a system, we'll achieve:

$$\begin{gathered}K_{1(x_{23})} = \left(\frac{\mu W_{Z1}}{2{\xi_{Z1}}^3 EA\delta_{mob}}\left[\frac{1}{EA} * F + \alpha\Delta T\right]\right)_{(x_{23})} \\ K_{2(x_{23})} = -\left(\frac{\mu W_{Z1}}{2{\xi_{Z1}}^3 EA\delta_{mob}}\left[\frac{1}{EA} * F + \alpha\Delta T\right]\right)_{(x_{23})}\end{gathered} \tag{35}$$

Algebraically manipulating ξ we can simplify equation (35) as:

$$K_{1_{(x_{23})}} = \left(\frac{1}{2}\sqrt{\frac{EA\delta_{mob}}{\mu W_{Z1}}}\left[\frac{1}{EA} * F + \alpha\Delta T\right]\right)_{(x_{23})}$$

$$K_{2_{(x_{23})}} = -\left(\frac{1}{2}\sqrt{\frac{EA\delta_{mob}}{\mu W_{Z1}}}\left[\frac{1}{EA} * F + \alpha\Delta T\right]\right)_{(x_{23})} \quad \textbf{(36)}$$

Or if we prefer:

$$K_{1_{(x_{23})}} = \left(\frac{1}{2}\sqrt{\frac{EA\delta_{mob}}{\mu W_{Z1}}}\,\varepsilon_{Total}\right)_{(x_{23})}$$

$$K_{2_{(x_{23})}} = -\left(\frac{1}{2}\sqrt{\frac{EA\delta_{mob}}{\mu W_{Z1}}}\,\varepsilon_{Total}\right)_{(x_{23})} \quad \textbf{(37)}$$

However, both solutions for K_1 and K_2, shown by equations (36) or (37), depend on the force acting at x_{23}. At this point, the value provided by Carr's solution is applied.

By the expressions shown in equation (36), it was foreseen that the impact of the rigid-plastic force value would be extremely small, once the force is divided by the axial stiffness. This prediction was later confirmed when the results were compared for K_1 and K_2 calculated with rigid-plastic and elastic-perfectly-plastic soils responses (the difference was 0.003%).